

EYE MOVEMENT PREDICTION BY OCULOMOTOR PLANT MODELING
WITH KALMAN FILTER 2003-2007

A dissertation submitted to
Kent State University in partial
fulfillment of the requirements for the
degree of Doctor of Philosophy

By
Oleg Vladimirovich Komogortsev

December, 2007

Dissertation written by

Oleg Vladimirovich Komogortsev

B.S., Volgograd State University, 2000

M.S., Kent State University, 2003

M.S., Volgograd State University, 2006

Ph.D., Kent State University, 2007

Approved by

Javed Khan

, Chair, Doctoral Dissertation Committee

Jonathan Maletic

, Members, Doctoral Dissertation Committee

Austin Melton

Jocelyn Folk

Jeff Wenstrup

Accepted by

Robert Walker

, Chair of Department of Computer Science

John Stalvey

, Dean, College of Arts and Sciences

TABLE OF CONTENTS

LIST OF FIGURES	vii
LIST OF TABLES.....	xi
ACKNOWLEDGMENT.....	xii
CHAPTER 1 INTRODUCTION.....	1
CHAPTER 2 RELATED WORK	5
2.1 DIRECT EYE GAZE INPUT	5
2.2 INTERACTIVE DISPLAYS	6
2.3 KALMAN FILTERING.....	8
2.4 OCULOMOTOR PLANT MODELING	9
CHAPTER 3 HUMAN VISUAL SYSTEM.....	11
3.1 DEFINITIONS OF BASIC EYE MOVEMENT TYPES	11
3.2 CONTROL.....	12
3.3 OCULOMOTOR PLANT MECHANICAL MODEL (OPMM).....	15
3.3.1 MUSCLE PROPERTIES.....	16
3.3.2 MUSCLE MECHANICAL MODEL (MMM).....	19
3.3.3 AGONIST MUSCLE MECHANICAL MODEL OF LATERAL RECTUS.....	21
3.3.4 ANTAGONIST MUSCLE MECHANICAL MODEL OF MEDIAL RECTUS ..	23

3.3.5	LENGTH TENSION RELATIONSHIP	25
3.3.6	FORCE VELOCITY RELATIONSHIP	29
3.3.7	NEURONAL CONTROL SIGNAL	30
3.3.8	ACTIVE STATE TENSION	34
3.3.9	OCULOMOTOR PLANT MECHANICAL MODEL EQUATIONS	38
3.3.10	EXAMPLE	42
CHAPTER 4	OCULOMOTOR PLANT KALMAN FILTER FRAMEWORK	44
4.1	BASICS OF KALMAN FILTERING	44
4.2	OCULOMOTOR PLANT KALMAN FILTER DESIGN	47
CHAPTER 5	DETECTION OF BASIC EYE MOVEMENT TYPES	57
5.1	VELOCITY-THRESHOLD IDENTIFICATION (I-VT)	57
5.2	SACCADE DETECTION BY THE TWO STATE KALMAN FILTER	58
CHAPTER 6	METHODOLOGY	60
6.1	EQUIPMENT	60
6.2	TEST MEDIA	60
6.3	PARTICIPANTS	63
6.4	EYE MOVEMENT PREDICTION MODELS	64
6.4.1	TWO STATE KALMAN FILTER (TSKF)	64
6.4.2	OCULOMOTOR PLANT MECHANICAL MODEL (OPMM)	65
6.4.3	OCULOMOTOR PLANT KALMAN FILTER (OPKF)	66
6.4.4	OCULOMOTOR PLANT KALMAN FILTER + (OPKF+)	68

6.5	EVALUATION	69
6.6	EYE MOVEMENT PREDICTION ACCURACY METRIC	70
CHAPTER 7 RESULTS.....		72
7.1	TEST VIDEO SET PERFORMANCE	72
7.2	EYE MOVEMENT PREDICTION RESULTS	76
7.2.1	FIXATIONS	79
7.2.2	SACCADES	81
7.2.3	PURSUICTS.....	83
7.2.4	ALL EYE MOVEMENTS COMBINED	85
7.2.5	STATISTICAL SIGNIFICANCE	86
7.3	EYE MOVEMENT PREDICTION DURING EYE TRACKING FAILURES	87
7.4	REAL-TIME PERFORMANCE	88
7.5	FUTURE IMPROVEMENT OF PREDICTION ACCURACY	89
CHAPTER 8 CONCLUSION		90
BIBLIOGRAPHY		92
GLOSSARY		97
APPENDIX A.....		98
A.1	AGONIST MUSCLE MECHANICAL MODEL OF LATERAL RECTUS.....	98
A.2	ANTAGONIST MUSCLE MECHANICAL MODEL OF MEDIAL RECTUS ..	99
A.3	OCULOMOTOR PLANT MECHANICAL MODEL – NEGATIVE AMPLITUDE	
SACCADES	101

A.4	OCULOMOTOR PLANT KALMAN FILTER	108
-----	--------------------------------------	-----

LIST OF FIGURES

Figure 1. Left eye diagram side view. Eye globe with six muscles.....	13
Figure 2. Left eye diagram front view. Arrows represent the direction of pulling forces created by each muscle.....	13
Figure 3. Muscle Mechanical Model. Red arrows represent directions of the forces...	20
Figure 4. Agonist Muscle Mechanical Model of Lateral Rectus. Arrows represent direction of the forces.....	22
Figure 5. Antagonist Muscle Mechanical Model of Medial Rectus. Arrows represent the direction of the forces.....	24
Figure 6. Force applied by the agonist and antagonist muscles to the eye globe for various eye positions and values of neuronal control signals.	27
Figure 7. Force (tension) is measured for the neuronal control signal represented by the position of unoperated eye and muscle length represented by the eye position of the operated eye.....	27
Figure 8. Neuronal control signal N_{AG} for the agonist muscle for a saccade with a 30° amplitude.	34
Figure 9. Active state tension inside of the agonist muscle during a saccade originating at the primary position, with an amplitude of 30°.....	36

Figure 10. The Oculomotor Plant Mechanical Model generating positive amplitude saccades. Arrows show the direction of forces for each component. F_{LR} , F_{MR} – active state tension; K_{LT} – length tension coefficient; K_{SE} – series elasticity coefficient; $\theta_{SE_MR}+\Delta\theta_{SE_MR}$, $\theta_{SE_LR}+\Delta\theta_{SE_LR}$ – length of the displacement of the series elasticity component of each muscle; $\theta_{LT_MR}+\Delta\theta_{LT_MR}$, $\theta_{LT_LR}-\Delta\theta_{LT_LR}$ – length of the displacement of the length tension component of each muscle; $\Delta\theta_{LT_LR}$, $\Delta\theta_{LT_MR}$ – velocity of change of the length tension component of the lateral and the medial recti; B_{AG} , B_{ANT} – damping coefficients for the agonist (the lateral rectus) and the antagonist (the medial rectus), $\Delta\theta$ – eye rotation; K_p – combined passive elasticity coefficient of the eye-orbit, both muscles and surrounding tissues; B_p – damping component coefficient for the viscosity of the eye-orbit and surrounding tissues. J is the rotational inertia of the eye globe.39

Figure 11. Force applied by the lateral and the medial recti to the eye globe during a saccade of -25° , originating at -5° of the primary eye position.....43

Figure 12. Car video snapshot.....61

Figure 13. Shamu video snapshot.62

Figure 14. Airplanes video snapshot.....63

Figure 15. Eye movement prediction by the TSKF model. The TSKF predicts eye movement trajectories during all eye movements.65

Figure 16. Eye movement prediction by the OPMM model. The TSKF predicts eye movement trajectories during all eye movements except saccades. The OPMM

predicts eye movement during saccades.	66
Figure 17. Eye movement prediction by the OPKF model. The TSKF predicts eye movement trajectories during all eye movements except saccades. The OPMM in the Kalman Filter form predicts eye movements during saccades.....	67
Figure 18. Eye movement prediction by the OPKF+ model. The TSKF predicts eye movement trajectories during all eye movements except saccades. The OPMM in the Kalman Filter form predicts eye movements during saccades +200 msec. after the end of each saccade.....	69
Figure 19. Average percentage of the eye position samples that belong to a specific eye movement type and the average percentage of Not Reported eye position samples.	73
Figure 20. Average fixation duration	73
Figure 21. Average saccade amplitude	74
Figure 22. Car video. The RMSE and RMSE standard deviations for four eye movement prediction models.	78
Figure 23. Shamu video. The RMSE and RMSE standard deviations for four eye movement prediction models.	78
Figure 24. Airplanes video. The RMSE and RMSE standard deviations for four eye movement prediction models.	79
Figure 25. Eye movement prediction by the Two State Kalman Filter during two eye tracking failures.....	88
Figure 26. Agonist Muscle Mechanical Model of Medial Rectus. Arrows represent the	

direction of the forces.....	102
Figure 27. Antagonist Muscle Mechanical Model of Lateral Rectus. Arrows represent	
Arrows represent the direction of the forces.	105
Figure 28. The Oculomotor Plant Mechanical Model generating negative amplitude	
saccades. Arrows show the direction of forces for each component. F_{LR} , F_{MR} – active	
state tension; K_{LT} – length tension coefficient; K_{SE} – series elasticity coefficient;	
$\theta_{SE_MR}-\Delta\theta_{SE_MR}$, $\theta_{SE_LR}-\Delta\theta_{SE_LR}$ – length of the displacement of the series elasticity	
component of each muscle; $\theta_{LT_MR}+\Delta\theta_{LT_MR}$, $\theta_{LT_LR}-\Delta\theta_{LT_LR}$ – length of the	
displacement of the length tension component of each muscle; $\Delta\theta_{LT_LR}$, $\Delta\theta_{LT_MR}$ –	
velocity of change of the length tension component of the lateral and the medial recti;	
B_{AG} , B_{ANT} – damping coefficients for the agonist (the lateral rectus) and the antagonist	
(the medial rectus), $\Delta\theta$ – eye rotation; K_p – combined passive elasticity coefficient of	
the eye-orbit, both muscles and surrounding tissues; B_p – damping component	
coefficient for the viscosity of the eye-orbit and surrounding tissues. J is the rotational	
inertia of the eye globe.	107
Figure 29. State vector prediction by the OPKF, during a saccade of a positive	
amplitude.	112

LIST OF TABLES

Table 1. Fixations. The RMSE values and the prediction accuracy improvement between the TSKF and the OPKF+ models.	80
Table 2. Saccades. The RMSE values and the prediction accuracy improvement between the TSKF and the OPKF+ models.	82
Table 3. Pursuits. The RMSE values and the prediction accuracy improvement between the TSKF and the OPKF+ models.	84
Table 4. All eye movements. The RMSE values and the prediction accuracy improvement between the TSKF and the OPKF+ models.	86
Table 5. t-test results.	87

ACKNOWLEDGMENT

I would like to thank my parents for their unending emotional support and their love for me. I also would like to thank my advisor, Dr. Javed Khan, who taught me how to accomplish the most challenging scientific goals. I would like to express my deepest thanks to Mrs. Sue Peti, for without her caring, this work would not be accomplished.

CHAPTER 1

Introduction

The human computer interaction world is rapidly growing. The community searches for new methods and inputs in order to provide a more natural, seamless process of communication between a human and a computer. Eye tracking technology successfully substitutes or enhances the already existing interaction methods and provides more natural, interactive environments. Due to the fact that interactive systems today are more frequently deployed in network environments that introduce various types of delay, accurate eye movement prediction will play a key role in the creation of more responsive and robust eye-guided systems

This Dissertation addresses the problem of horizontal eye movement prediction within a specific time interval. To solve this problem the Oculomotor Plant Kalman Filter (OPKF) framework was developed. The OPKF framework consists of two components that predict future eye movements: an Oculomotor Plant Mechanical Model (OPMM) and a Kalman Filter. The OPMM is a mechanical model of an eye that takes into account eye's anatomical properties. The model developed in this Dissertation is based upon Bahil's model (Bahill, Development, validation and sensitivity analyses of human eye movement models, 1980). Bahil's model only generates saccades that start from the primary eye position and are developed in one

direction. The first contribution of this Dissertation is an eye mechanical model that is capable of generating saccades that start from any horizontal eye position and progress in any direction in a horizontal plane. The second contribution of this Dissertation is the representation of the eye mechanical model in a Kalman Filter form. This representation enables continuous real-time eye movement prediction. The third contribution of this Dissertation is formulating of a function that connects a chi square test value, which is created by the observed eye velocity and the velocity predicted by a Kalman Filter, to the future saccade's amplitude.

Direct eye gaze input and interactive displays are areas of Human Computer Interaction domain that will benefit the most from accurate eye movement prediction.

Interactive displays use eye tracker measured eye position data to increase resolution, to raise image update rate and provide a more detailed simulation of a particular phenomenon within a specified region of interest. This approach allows to achieve both a bit-rate and computational burden reduction without changing the perceived quality of the display. An example of an interactive display can be presented with a perceptual compression which presents an image to the viewer with high quality in the region where a viewer is looking and reduces the quality in the periphery. This scheme reduces the bit-rate of a video stream by 50% without the loss of perceived quality (Komogortsev & Khan, Predictive Perceptual Compression for Real Time Video Communication, 2004). In the scenarios in which perceptual compression is performed in a network environment transmission delays are inevitable. Those delays are 20 msec. and longer. During a delay fast eye movements (saccades, smooth

pursuits) can move the eye position away from the region where high visual quality is maintained, thereby increasing the probability that the attention will be directed to the compressed part of the image which is of lower quality. Eye movement prediction will allow a future attention span to be contained within a specified window, thus placing a high quality region into the area of the future attention focus (Komogortsev & Khan, Predictive Perceptual Compression for Real Time Video Communication, 2004),(Komogortsev & Khan, Perceptual Attention Focus Prediction for Multiple Viewers in Case of Multimedia Perceptual Compression with Feedback Delay, 2006),(Khan & Komogortsev, 2006),(Komogortsev & Khan, Perceptual Multimedia Compression based on the Predictive Kalman Filter Eye Movement Modeling, 2007).

Eye gaze data can be used as a direct input to a computer (Jacob, 1995),(Salvucci & Anderson, Intelligent gaze-added interfaces, 2000),(Partala, Jokiniemi, & Surakka, 2001). This enables eye movements to be interpreted as commands to the interface components. Accurate eye movement prediction will increase the responsiveness of every system that uses eye-gaze-based commands. As an example, prediction of fast eye movement (saccade) will allow placing system's response to the area targeted by a saccade, anticipating a user's intentions.

The main objective of this Dissertation was to design a framework that predicts an eye movement trajectory within a specified time interval, detects saccades, provides an eye position signal during periods when the eye tracking fails, and has a real-time performance.

The structure of the Dissertation is as follows: CHAPTER 2 discusses the previous work relevant to the topics presented in this Dissertation; CHAPTER 3 presents insight into eye movement neuronal control and eye mechanical modeling; CHAPTER 4 introduces the basics of Kalman Filtering and a representation of an eye mechanical model in a Kalman Filter form; CHAPTER 5 presents two algorithms for the eye movement type detection and a method of predicting saccade amplitude based on a statistic generated by a Kalman Filter; CHAPTER 6 presents four eye movement prediction models and the setup parameters used to test these models; CHAPTER 7 presents the accuracy results achieved by four prediction models; CHAPTER 8 presents the conclusion of the work developed in this Dissertation.

CHAPTER 2

Related Work

There are two areas where eye movement prediction is critical: direct eye gaze interaction and interactive displays. The beginning of this chapter presents past research work that is related to those areas. The Kalman Filter is an integral part of the eye movement prediction framework developed in this Dissertation. Thus the research in the Kalman Filtering domain that is related to eye movements is presented. One of the core issues presented in this Dissertation is a mechanical modeling of the human eye. The previous research related to this topic is presented last.

2.1 Direct Eye Gaze Input

Today direct eye gaze input is mainly used as an assistive technology for motion impaired people, but it is anticipated that in the future, eye-gaze-based input will be added to almost every computing device.

Jacob has developed an application, where he tested the effectiveness of the eye gaze input (Jacob, 1995). Different interface actions were triggered by specific eye fixation durations. Jacob has reported that an eye gaze input accuracy was comparable to a touch screen display rather than a mouse, but the system provided an impression of

responding to the user's intention rather than explicit input.

Komogortsev has implemented an eye gaze-based interface that used communication tokens created by the basic eye movement types for interaction. The interface was implemented for the World of Warcraft computer game (Komogortsev, World of Warcraft Percept Interface, 2007). Target selection in game was more fluid with the eye gaze input than with a mouse input. Small objects were hard to select and certain commands (spell selection, avatar movement) were triggered by voice commands.

Murtagh et. al. (Murtagh, Farid, & Starck, 2002) have built an eye gaze controlled mouse application that allowed accurate interaction with relatively large components of the interface. The limitation on accuracy of the eye tracking imposed the size constrains on the interface components. The larger was the size of the interface components the higher was the accuracy of the eye gaze input.

To the best of my knowledge the eye movement prediction was not investigated by the researchers studying the direct eye gaze input.

2.2 Interactive Displays

The most popular application of interactive display today lies in the area of perceptual compression. Perceptual compression uses eye gaze position information to compress a visual source without reducing its perceptual quality. Eye movement prediction allows the use of perceptual compression when multimedia is transmitted

through a network.

Interactive display research was performed for still images by Tsumura et. al. (Tsumura, Endo, Haneishi, & Miyake, 1996). Part of the image where a viewer's attention was directed was transmitted first and the periphery of the image was transmitted next.

Wang and Bovik have presented a foveated algorithm to compress still images in (Wang & Bovik, 2001).

Komogortsev and Khan researched a single viewer eye gaze-based real-time video compression in a network environment (Komogortsev & Khan, Predictive Perceptual Compression for Real Time Video Communication, 2004),(Komogortsev & Khan, Perceptual Multimedia Compression based on the Predictive Kalman Filter Eye Movement Modeling, 2007). Estimated compression achieved by this scheme was 50%. The multi viewer scenario was examined in (Komogortsev & Khan, Perceptual Attention Focus Prediction for Multiple Viewers in Case of Multimedia Perceptual Compression with Feedback Delay, 2006). The results indicated that perceptual multimedia compression is possible for multiple people. Several attention prediction models were developed by Komogortsev and Khan (Khan & Komogortsev, 2006) to increase perceptual compression effectiveness by merging a real-time scene content analysis and supplemental eye tracking data.

In regard to the interactive displays the eye movement prediction was considered in Komogortsev's and Khan's research (Komogortsev & Khan, Predictive Perceptual Compression for Real Time Video Communication, 2004),(Komogortsev & Khan,

Perceptual Attention Focus Prediction for Multiple Viewers in Case of Multimedia Perceptual Compression with Feedback Delay, 2006),(Khan & Komogortsev, 2006),(Komogortsev & Khan, Perceptual Multimedia Compression based on the Predictive Kalman Filter Eye Movement Modeling, 2007) in a form of Perceptual Attention Window – a region of interest that was designed to contain future eye fixations.

2.3 Kalman Filtering

Eye movement detection by a Kalman Filter was proposed by Sauter et. al. (Sauter, J., Di Renzo, & Vomscheid, 1991). Sauter used the innovations generated by a Kalman Filter to identify saccades. The Hinkley algorithm (Hinkley, 1971) was used to detect the onset and the end of each saccade. Saccade detection was done offline.

Grindiger (Grindinger, 2006) used a Kalman Filter to identify different eye movement types following the idea proposed by Sauter. Gridinger's implementation used a mouse movement generated signal as a testbed for saccade detection. The saccade detection parameters proposed by Gridinger allowed the construction of a well-behaved saccade detection filter within the limitations of his setup.

2.4 Oculomotor Plant Modeling

The first human saccadic eye movement system was modeled by Westheimer in (Westheimer, 1954). He modeled saccades by a linear second order system. His model

produced correct eye position trajectories for saccades of 20°.

Robinson has proposed a model with a pulse-step control neuronal signal sent to the eye muscles in (Robinson, Models of the saccadic eye movement control system, 1973). Robinson model was a fourth order system that generated correct eye movements trajectories for the saccades of various sizes, but with eye-velocity profiles that did not match the human data.

Bahil et. al. have presented a linear homeomorphic model that was represented by a sixth order system (Bahill, Latimer, & Troost, Linear homeomorphic model for human movement, 1980). With proper selection of parameters the model was capable of generating horizontal saccades of various amplitudes with correct velocity profiles. Bahill's model was capable of generating saccades in only one direction and those saccades originated only in the primary eye position (eye looking straight ahead). The OPFK framework described in this Dissertation modifies Bahill's model in a way that makes it possible to generate saccades in both directions and allows saccade initialization from any eye position.

Martin and Schovanec have created a non-linear ten order system in (Marin & Schovanec, 1999), removing some artifacts that remained in Bahill's model due to linearization, but their model still had positional and directional limitation inherited from the Bahill's model.

From the eye movement prediction point of view all models described above can be used for the eye movement trajectory prediction during a saccade of a known

amplitude originating in the primary eye position.

CHAPTER 3

Human Visual System

This Dissertation defines eye movement prediction as a prediction of eye movement trajectories during various eye movement types. This Chapter defines basic eye movement types and explains why they are important to human vision. The eye mechanical model presented in this Chapter is one of the most important tools that will be used to improve eye movement prediction accuracy. Neuronal control and mechanical modeling of the muscle properties will be discussed.

3.1 Definitions of Basic Eye Movement Types

(i) Fixation: - “an eye movement which stabilizes the retina over a stationary object of interest” (Duchowski, 2003). Eye fixations are accompanied by drift, small involuntary saccades and tremor. A human’s eye perceives the highest quality picture during an eye fixation. Eye fixation duration usually ranges from 100 msec. to 600 msec. with eye velocity not exceeding 100 deg/sec during a fixation.

(ii) Saccades: - “rapid eye movements used in repositioning the fovea to a new location in the visual environment” (Duchowski, 2003). Usually saccades transition the Human Visual System (HVS) from one eye fixation to another. The HVS is blind

during a saccade (Shebilske & Fisher, 1983). Saccade duration range from 30 msec. to 120 msec., with eye velocities going above 300 deg/sec.

(iii) Smooth pursuit: - a neye movement that develops when the eyes are tracking a moving visual target. It consists of two components: a slowly varying motion component plus a saccadic component. This saccadic component occurs occasionally as a correction mechanism for the eye when the current eye position is not accurate with respect to the moving object (Yanoff & Durker, 1999). The slowly varying motion component of the smooth pursuit keeps the retina stable over the moving object and high quality visual data is perceived during this period. The quality of vision varies during smooth pursuit eye movements depending on the eye and object velocities, with the most comfortable velocities being < 200 deg/sec for the HVS to ensure tracking. Some elements of pursuit are maintained when an object velocity is approximately 350-400 deg/sec.

3.2 Control

The eye globe rotates in its socket through the use of six muscles as it is presented in Fig. 1. These six muscles are: the medial and the lateral recti – the muscles responsible for horizontal eye movements; superior and inferior recti – the muscles responsible for vertical eye movements; superior and inferior oblique – the muscles responsible for eye rotations around its primary axis of sight; and vertical eye movements. The eye rotations accomplished by these six muscles are presented in Fig.

2.

Left eye diagram side view

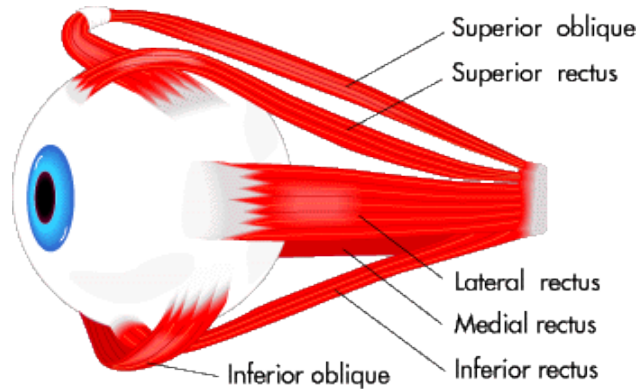


Fig. 1. Left eye diagram side view. Eye globe with six muscles.

Left eye diagram front view

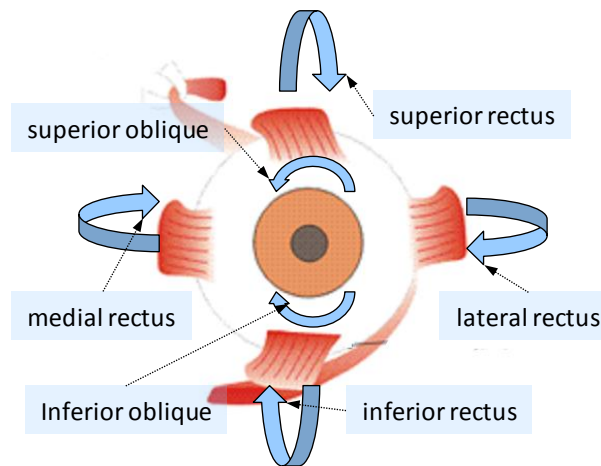


Fig. 2. Left eye diagram front view. Arrows represent the direction of pulling forces created by each muscle.

The Brain sends a neuronal control signal to each muscle to direct the muscle to perform its work. A neuronal control signal is anatomically implemented as a neuronal discharge that is sent through a nerve to a designated muscle from a specific part of the

brain (Sparks, 2002). The frequency of this discharge determines the level of muscle innervation and results in a specific amount of work that a muscle can perform. Specifically, a neuronal control signal is sent to the medial rectus through the abducens nerve and to the lateral rectus through the oculomotor nerve. A neuronal control signal is sent to the superior and inferior recti through the oculomotor nerve. A neuronal control signal is sent to the superior oblique through the trochlear nerve and to the inferior oblique through the oculomotor nerve.

During saccadic eye movements, a saccade trajectory can be separated into horizontal and vertical component. The neuronal control signal for the horizontal and the vertical components are generated by different parts of the brain. The control signal for the horizontal component is generated by the premotor neurons in the pons and medulla (Sparks, 2002) and executed by the medial and the lateral recti muscles. The rostral midbrain generates a neuronal control signal for the vertical eye movement component (Sparks, 2002). The vertical eye movement component is executed by the superior, the inferior recti and the superior, the inferior oblique. During saccades the neuronal control signal for each muscle resembles a pulse-step function. The eye position during the onset of a saccade, the saccade's amplitude and direction define pulse and step parameters of the control signal. Once the parameters of the neuronal control signal are calculated by the brain, the control signal is sent as a neuronal discharge at the calculated frequency.

During eye fixations neuronal discharge is performed at a constant rate that is

linearly related to the eye position.

3.3 Oculomotor Plant Mechanical Model (OPMM)

The oculomotor plant is represented by a mechanical model composed of six muscles attached to a globe of ice representing the eye sphere. This Dissertation works only with the horizontal component of the oculomotor plant that consists of the lateral (the muscle that is closer to the ear) and the medial (the muscle that is closer to the nose) recti, eye globe and surrounding tissues. The eye globe's radius is 11mm. The lateral and the medial recti are modeled through a system of mechanical components described in latter sub-sections. Either the lateral or the medial recti can play the role of the agonist or the antagonist. The agonist muscle pulls the eye globe in the required direction and the antagonist muscle resists the pull.

The subscript notation will identify the agonist parameters with AG and the antagonist parameters with ANT. The subscript notation will identify with LR the parameters that belong to the lateral rectus and with MR the parameters that belong to the medial rectus. Parameters without those subscripts are identical to both types of muscles.

The horizontal OPMM is capable of producing only horizontal eye movements and only during saccades. This Dissertation modifies the horizontal OPMM presented by Bahill (Bahill, Development, validation and sensitivity analyses of human eye movement models, 1980). There are two major contributions added to Bahill's model:

1) the ability to start a saccade from any horizontal eye position, and 2) the ability to make a saccade in any horizontal direction.

Assumptions and definitions.

The OPMM is integrated into a Kalman Filter only during saccades; prediction during all other eye movements is done by a Two State Kalman Filter (TSKF), described in Section 4.2.

Each saccade is defined by its onset time, stop time, amplitude, direction and the eye position during the onset of the saccade.

The OPMM as developed is presented using the anatomy of the right eye, though the model can be easily modified to work for the anatomy of the left eye as well.

Positive amplitude saccades are defined as saccades that move the right eye to the right. Positive amplitude saccades are performed by the lateral rectus as the agonist and by the medial rectus as the antagonist.

Negative amplitude saccades are defined as saccades that move the right eye to the left. Negative amplitude saccades are performed by the lateral rectus as the antagonist and by the medial rectus as the agonist.

3.3.1 Muscle Properties

A muscle is a very complex structure (Wilkie, 1976). The Muscle Mechanical Model (MMM) can be represented through several components. These components are the following: passive elasticity, active state tension, a series elasticity, a length-tension

component and a force velocity relationship (Bahill, Development, validation and sensitivity analyses of human eye movement models, 1980),(Hill, 1938),(Collins, 1975),(Robinson, Omeara, Scott, & Collins, 1969).

Passive Elasticity: Each body muscle in the rest state is elastic. The rested muscle can be stretched by applying force. The muscle extension is proportional to the force applied. The passive elasticity results largely from the meshwork of connective tissue within the muscle, whose fibers become progressively taut when the muscle is stretched (Wilkie, 1976). The passive muscle component is non linear, but in this Dissertation it is modeled as an ideal linear spring. The numerical value for the spring coefficient representing passive elasticity was estimated by Collins (Collins, 1975).

Active State Tension: Each muscle produces active state tension when it is stimulated. When stimulated by a single wave of neurons a muscle twitches then relaxes. A muscle goes into the tetanic state, when it is stimulated by neurons at a specific frequency continuously (Wilkie, 1976). As was mentioned in Section 3.2, the frequency of the neuronal discharge is determined by the neuronal control signal parameters estimated by the brain. When a tetanic stimulation occurs, a muscle develops tension, trying to contract. The resulting tension is called the active state tension. The intensity of the active state tension depends upon the frequency of the neuronal discharge. An ideal force generator component is used in the MMM to represent active state tension. Section 3.3.8 provides an additional description of the active state tension.

Length Tension Relationship: The tension that a muscle develops as a result of neuronal stimulation partially depends on its length. Usually the tension in a significantly contracted muscle is less than the maximum tension that a muscle is capable of creating at its optimal length. A length tension effect occurs due to the following reasons: when a stimulated muscle is lengthened considerably, the area of overlap of thick and thin filaments (anatomical components responsible for muscle contraction) diminishes and as a result the muscle's active state tension diminishes as well. When a stimulated muscle is shortened considerably the thin and thick filaments interfere with the series elastic elements of the muscle, absorbing part of the tension developed, thus reducing the overall active state tension. Additionally when a muscle is significantly shortened, neuronal stimulation does not reach inner muscle contractile fibers (Wilkie, 1976). Section 3.3.5 provides experimental measurement of the length tension relationship.

Series Elasticity: The existence of the series elasticity component was demonstrated by Levin and Wyman (Levin, 1927) in an experiment in which a weight was hung from a muscle, and the muscle was stimulated tetanically. The weight was then released from the muscle. The muscle contracted and lengthened again, and the muscle length and force were recorded as functions of time. The data was analyzed and the conclusion was made that there are a spring-like components inside a muscle between contractile components and the body tissues. The series elasticity is in series with the active force generator and hence the name. Anatomically, spring elasticity components are located on the tendon and in myosin and in the actin bridges of the muscle fibers. In

the MMM series elasticity component is modeled as an ideal linear spring.

Force Velocity Relationship: This relationship shows that a muscle is capable of producing larger forces at lower velocities. This dependency of force upon velocity varies for different levels of a neuronal control signal and depends on whether a muscle shortens or being stretched. It is believed that the force velocity relationship exists due to the different rates of chemical reactions inside a muscle at various length-changing velocities (Wilkie, 1976). Section 3.3.6 provides formulas describing the force velocity relationship.

3.3.2 Muscle Mechanical Model (MMM)

The lateral rectus MMM is presented in Fig. 3. In this Figure the eye globe is depicted in its primary position in the stationary state. T_{LR} is the force applied by the lateral rectus to the eye globe. N_{LR} is a neuronal control signal. F_{LR} is the active state tension inside of the muscle; it is modeled as an ideal force generator. The series elasticity component is modeled as a linear spring $K_{SE}\theta_{SE_LR}$, where θ_{SE_LR} is the displacement of the spring and K_{SE} is the spring's coefficient. The length tension component is modeled as a linear spring that adds its force to the active state tension. The force created by the length tension spring is $K_{LT}\theta_{LT_LR}$, where θ_{LT_LR} is the displacement of the spring and K_{LT} is the spring's coefficient. θ_{LT} is the combined displacement of the series elasticity and length tension component $\theta_{LR}=\theta_{LT_LR}+\theta_{SE_LR}$. In the MMM the active state tension and length tension components move

simultaneously.

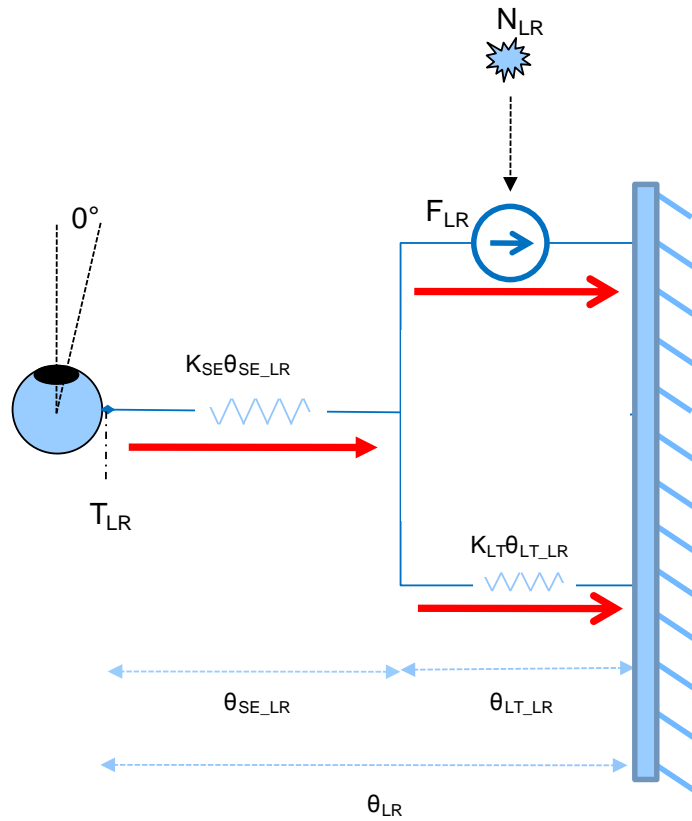


Fig. 3. Muscle Mechanical Model. Red arrows represent directions of the forces.

The next two subsections describe the changes in the MMM when the eye globe is rotating. The first case presents a MMM of the agonist muscle. The second case presents a MMM of the antagonist muscle.

3.3.3 Agonist Muscle Mechanical Model of Lateral Rectus

The agonist muscle contracts, rotates the eye globe and stretches the antagonist muscle. Assuming that the lateral rectus plays the role of the agonist we can present the

MMM of the agonist muscle pulling the eye-globe in the positive direction in Fig. 4. The original length of the displacement in the series elasticity spring and the length tension spring added together is θ_{LR} . Considering that the right eye moves to the right by $\Delta\theta$ degrees, the original displacement θ_{LR} is reduced making the resulting displacement $\theta_{LR}-\Delta\theta$. The displacement $\Delta\theta$ is $\Delta\theta=\Delta\theta_{SE_LR}-\Delta\theta_{LT_LR}$. Muscle contraction expands the series elastic component making the resulting displacement $\theta_{SE_LR}+\Delta\theta_{SE_LR}$. Muscle contraction shortens the length tension component making the resulting displacement $\theta_{LT_LR}-\Delta\theta_{LT_LR}$. The damping component modeling the force velocity relationship $B_{AG}\Delta\dot{\theta}_{LT_LR}$ resists the muscle contraction. The amount of resistive force produced by the damping component is based upon the velocity of contraction of the length tension component.

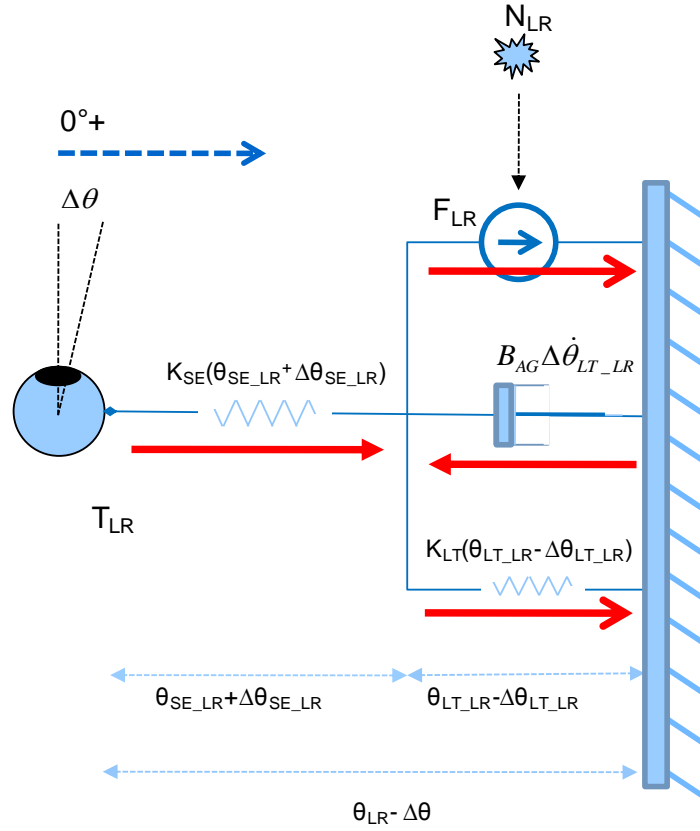


Fig. 4. Agonist Muscle Mechanical Model of Lateral Rectus. Arrows represent direction of the forces.

Using Fig. 4, we can write the equation of force with which the part of the diagram responsible for contraction (active state tension, damping component, length tension component) pulls the series elasticity component.

$$T_{LR} = F_{LR} + K_{LT}(\theta_{LT_LR} - \Delta\theta_{LT_LR}) - B_{AG}\Delta\dot{\theta}_{LT_LR} \quad (1)$$

Resisting the contraction, the series elasticity component propagates the contractile force by pulling the eye globe with the same force T_{LR} .

$$T_{LR} = K_{SE}(\theta_{SE_LR} + \Delta\theta_{SE_LR}) \quad (2)$$

Equations 1 and 2 can be used to calculate the force T_{LR} in terms of the eye rotation $\Delta\theta$, and displacement $\Delta\theta_{LT_LR}$ of the length tension component of the muscle.

$$T_{LR} = \frac{K_{SE}\hat{F}_{LR}}{K_{SE} + K_{LT}} - \frac{\Delta\theta K_{SE}K_{LT}}{K_{SE} + K_{LT}} - \hat{B}_{AG}\Delta\dot{\theta}_{LT_LR} \quad (3)$$

$$T_{LR} = K_{SE}(\Delta\theta_{LT_LR} - \Delta\theta) \quad (4)$$

The transition of Equations 1 and 2 into Equations 3 and 4 is described in Appendix A.1.

3.3.4 Antagonist Muscle Mechanical Model of Medial Rectus

The antagonist muscle is stretched by the agonist pull. Assuming that the medial rectus plays the role of the antagonist, the MMM of the medial rectus being stretched in the positive direction can be represented in Fig. 5. Originally the length of the displacement in the series elasticity and the length tension springs added together is θ_{MR} . θ_{MR} and increases when the eye moves to the right by $\Delta\theta$, making the resulting displacement $\theta_{MR} + \Delta\theta$. Both length tension and series elasticity components lengthen as a result of the agonist pull. The eye rotation $\Delta\theta$ can be split into the displacement of the series elasticity component and the length tension component: $\Delta\theta = \Delta\theta_{SE_MR} + \Delta\theta_{LT_MR}$. The resulting displacement for the series elasticity component is $\theta_{SE_MR} + \Delta\theta_{SE_MR}$ and for the length tension component is $\theta_{LT_MR} + \Delta\theta_{LT_MR}$. The damping component modeling the force velocity relationship $B_{ANT}\Delta\dot{\theta}_{LT_MR}$ resists the muscle stretching. The amount of resistive force is based upon the velocity of stretching of the length

tension component.

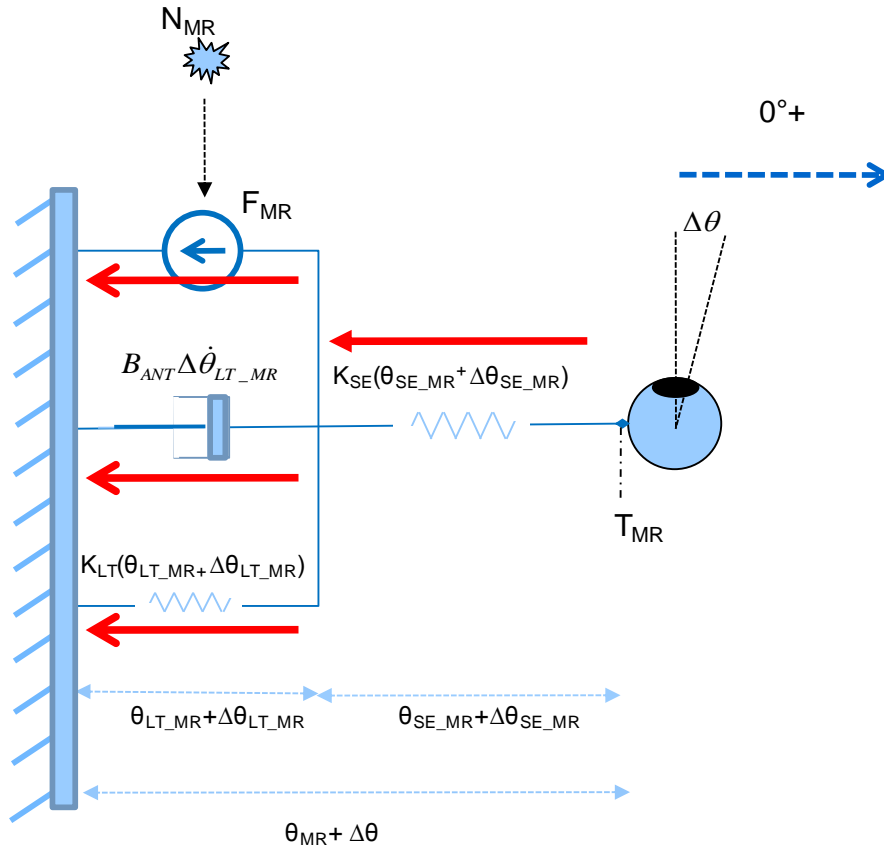


Fig. 5. Antagonist Muscle Mechanical Model of Medial Rectus. Arrows represent the direction of the forces.

Using Fig. 5, we can write the equation of force with which the part of the diagram responsible for the contraction (active state tension, damping component, length tension component) pulls the series elasticity component.

$$T_{MR} = -F_{MR} - K_{LT}(\theta_{LT_MR} - \Delta\theta_{LT_MR}) - B_{ANT}\Delta\dot{\theta}_{LT_MR} \quad (5)$$

Resisting the contraction the series elasticity component propagates the contractile force by pulling the eye globe with the same force T_{MR} .

$$T_{MR} = -K_{SE}(\theta_{SE_MR} + \Delta\theta_{SE_MR}) \quad (6)$$

Equations 5 and 6 can be used to calculate the force T_{MR} in terms of the eye rotation $\Delta\theta$, and displacement $\Delta\theta_{LT_LR}$ in the length tension component of the muscle.

$$T_{MR} = -\frac{K_{SE}\hat{F}_{MR}}{K_{SE} + K_{LT}} - \frac{\Delta\theta K_{SE}K_{LT}}{K_{SE} + K_{LT}} - \hat{B}_{ANT}\Delta\dot{\theta}_{LT_MR} \quad (7)$$

$$T_{MR} = -K_{SE}(\Delta\theta - \Delta\theta_{LT_MR}) \quad (8)$$

The transition of Equations 5 and 6 into Equations 7 and 8 is described in the Appendix A.2.

3.3.5 Length Tension Relationship

In the length tension measurement experiments reported by Robinson et. al. (Bahill, Latimer, & Troost, Linear homeomorphic model for human movement, 1980), the force applied by each muscle to the eye globe was measured at the tendon – the place where a muscle connects to the eye globe. These force measurements were taken during a strabismus surgery – a type of surgery in which muscles are detached and then reattached to the eyeball to correct muscle dislocation. During the surgery, before the muscle was reattached to the eye globe, the patient was instructed to look at certain targets with his unoperated eye while the corresponding muscle of the operated eye was stretched to correspond to the angular position of the unoperated eye. The angular position of the unoperated eye represented the value of the neuronal control signal while the angular position of the operated eye represented the length of the muscle. For

example, when the operated eye was held 20° temporal of the primary position and the subject was asked to look at a target 10° temporal of the primary position with his unoperated eye, a force of 24 grams was recorded in the lateral rectus of the operated eye. Fig. 7 presents the diagram of the measurement. Following the experiment design, muscle forces were measured for various muscle lengths, values of neuronal control signal and muscle roles (agonist, antagonist) (Robinson (Robinson, Omeara, Scott, & Collins, 1969)). Fig. 6 presents linearized results of those measurements. Part of Fig. 6 is copied from Bahill (Bahill, Development, validation and sensitivity analyses of human eye movement models, 1980).

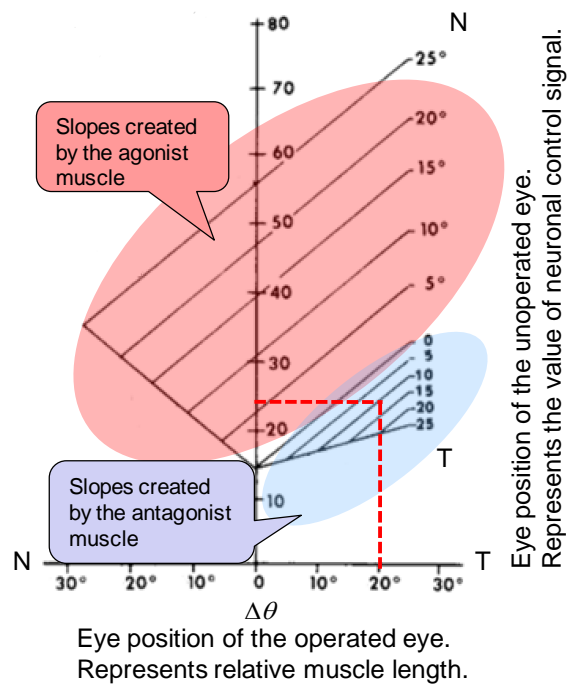


Fig. 6. Force applied by the agonist and antagonist muscles to the eye globe for various eye positions and values of neuronal control signals.

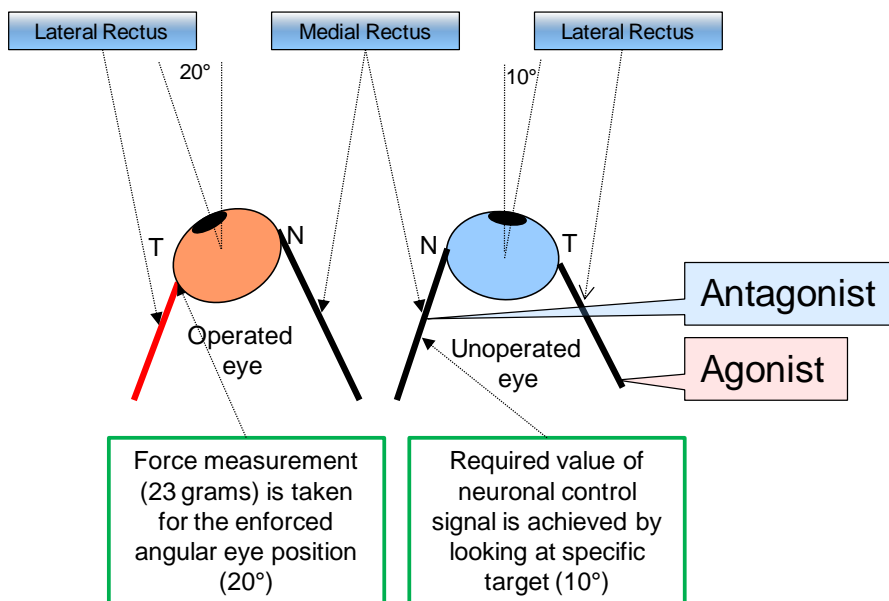


Fig. 7. Force (tension) is measured for the neuronal control signal represented by the position of unoperated eye and muscle length represented by the eye position of the operated eye.

The length tension slopes of Fig. 6 are created by Equations 3 and 7. Taking into consideration that the value of K_{SE} was measured by Collins (Collins, 1975) to be 2.5 grams of tension per degree and $K' = \frac{K_{SE}K_{LT}}{K_{LT}+K_{SE}}$ represented by the slopes of Fig. 6 equals to 0.8 grams of tension per degree, K_{LT} can be calculated as 1.2 grams of tension per degree.

The values of muscle forces required to hold an eye in a state of regular eye fixation by the agonist and the antagonist muscles were calculated by Bahill (Bahill, Development, validation and sensitivity analyses of human eye movement models, 1980) as:

$$T_{AG_FIX}(\theta) = 14 + 0.8|\theta| \text{ grams} \quad (9)$$

$$T_{ANT_FIX}(\theta) = 14 + 0.3|\theta| \text{ grams} \quad (10)$$

where θ is the eye position measured in degrees. $|\theta|$ is the absolute value of θ .

During a fixation state the active state tension \hat{F} in Equations 3 and 7 is assumed to be same as the neuronal control signal sent to the muscle. The value of the neuronal control signal during a fixation state for each muscle role can be calculated using the slopes of Fig. 6:

$$N_{AG_FIX}(\theta) = (20.6 + 2.37|\theta|) \text{ grams} \quad (11)$$

$$N_{ANT_FIX}(\theta) = \begin{cases} (20.6 - 0.74|\theta|) & \text{if } |\theta| \leq 28^\circ \\ 0 & \text{if } |\theta| > 28^\circ \end{cases} \quad (12)$$

It is obvious that the neuronal control signal cannot be negative which is why the neuronal control signal for the agonist muscle is assumed to be zero for angular eye

positions of more than 28°. Though the values of the neuronal control signal in Equations 11 and 12 are presented in grams, they can be converted into the units of spikes/sec. The conversion between these two units is done by a constant with a value of 0.48 grams-sec per spike.

3.3.6 Force Velocity Relationship

A force velocity relationship takes place when a stimulated muscle changes its length under the load. Hill (Hill, 1938) formulated this equation to describe a force-velocity relationship:

$$V = \frac{(F_0 - T)B}{(T + A)} \quad (13)$$

In this equation V is a muscle's length changing velocity, T is the muscle's force, F_0 is the isometric force representing the muscle's force measured at zero velocity, at the length where the muscle is capable of exerting maximum force. A and B are constants connected to the values of the neuronal control signal.

Equation 13 can be rearranged as:

$$T = F_0 - \frac{(F_0 + A)}{(B + V)} V \quad (14)$$

From Equation 14 it can be seen that the higher is the muscle's length changing velocity, the less force the muscle is capable of generating. To rephrase, the damping component inside the MMM offers more resistance at higher velocities.

It should be noted that the force velocity relationship is different for the contracting

muscle and for the muscle that is being stretched. The force created by dashpots representing the force velocity relationship can be linearly approximated for each muscle. Bahill (Bahill, Development, validation and sensitivity analyses of human eye movement models, 1980) suggests using the following dashpot values for the shortening (agonist) muscle represented by Equation 3 and the lengthening (antagonist) muscle represented by Equation 7:

$$\hat{B}_{AG} = 0.04 \text{ grams-sec/}^\circ \quad (15)$$

$$\hat{B}_{ANT} = 0.02 \text{ grams-sec/}^\circ \quad (16)$$

3.3.7 Neuronal Control Signal

Each saccade is generated by a neuronal control signal that looks like a pulse step function (Section 3.2). The neuronal control signal can be presented by the following equations:

$$N_{AG_sac}(t) = \begin{cases} N_{AG_sac_start}, & t_{sac_start} \leq t < t_{AG_sac_pulse_start} \\ N_{AG_sac_pulse}, & t_{AG_sac_pulse_start} \leq t < t_{AG_sac_pulse_end} \\ N_{AG_sac_end}, & t_{AG_sac_pulse_end} \leq t < t_{sac_end} \end{cases} \quad (17)$$

$$N_{ANT_sac}(t) = \begin{cases} N_{ANT_sac_start}, & t_{sac_start} \leq t < t_{ANT_sac_pulse_start} \\ N_{ANT_sac_pulse}, & t_{ANT_sac_pulse_start} \leq t < t_{ANT_sac_pulse_end} \\ N_{ANT_sac_end}, & t_{ANT_sac_pulse_end} \leq t < t_{sac_end} \end{cases} \quad (18)$$

t_{name} constants present time parameters for each type of muscle and action phase. t is the time elapsed from the beginning of the saccade. The OPMM developed in this Dissertation uses the time constants values presented below.

$$t_{sac_start} = 0$$

$$t_{sac_end} = (2.2 * |\theta_{sac_amp}| + 21) msec.$$

θ_{sac_amp} is the amplitude of the saccade measured in degrees, $t_{sac_end} - t_{sac_start}$ is the duration of the saccade, calculated by the formula proposed by Carpenter in (Carpenter, 1977).

The agonist muscle related time constants are:

$$t_{AG_sac_pulse_start} = t_{sac_start} + 3 msec.$$

$$t_{AG_sac_pulse_end} = (t_{AG_sac_pulse_start} + |\theta_{sac_amp}| + 10) msec.$$

The antagonist muscle related time constants are:

$$t_{ANT_sac_pulse_start} = t_{sac_start}$$

$$t_{ANT_sac_pulse_end} = (t_{AG_sac_pulse_start} + |\theta_{sac_amp}| + 16) msec.$$

The value representing the width of the antagonist pulse ($t_{ANT_sac_pulse_end} - t_{ANT_sac_pulse_start}$) is selected as a result of physiological measurements that indicated that the agonist pulse starts 3 msec. after the start of the antagonist pulse and ends 3 msec. before the end of the antagonist pulse.

The agonist and antagonist muscle neuronal control signal parameters $N_{AG_sac_start}$,

$N_{ANT_sac_start}$, $N_{AG_sac_end}$, $N_{ANT_sac_end}$, that are going to be presented next, are proposed in this Dissertation to acknowledge the neuronal control signal values before and after a saccade.

$$N_{AG_sac_start} = \begin{cases} N_{AG_FIX}(\theta_{sac_start}), & \text{if muscle was agonist prior to saccade} \\ N_{ANT_FIX}(\theta_{sac_start}), & \text{if muscle was antagonist prior to saccade} \end{cases}$$

$$N_{AG_sac_pulse} = \begin{cases} 11 + |\theta_{sac_amp}|, & \text{if } \theta_{sac_amp} \leq 11^\circ \\ 160 + 2|\theta_{sac_amp}|, & \text{if } \theta_{sac_amp} > 11^\circ \end{cases}$$

$$N_{AG_sac_end} = \begin{cases} N_{AG_FIX}(\theta_{sac_end}), & \text{if muscle became agonist after saccade} \\ N_{ANT_FIX}(\theta_{sac_end}), & \text{if muscle became antagonist after saccade} \end{cases}$$

θ_{sac_amp} - saccade amplitude, θ_{sac_start} - the angular horizontal eye position coordinate at the beginning of a saccade, θ_{sac_end} - the angular eye position coordinate at the end of a saccade. $N_{AG_FIX}(\theta_{sac_end})$ and $N_{ANT_FIX}(\theta_{sac_end})$ are functions calculated by Equations 11 and 12.

The antagonist muscle related neuronal control signal parameters are:

$$N_{ANT_sac_start} = \begin{cases} N_{AG_FIX}(\theta_{sac_start}), & \text{if muscle was agonist prior to saccade} \\ N_{ANT_FIX}(\theta_{sac_start}), & \text{if muscle was antagonist prior to saccade} \end{cases}$$

$$N_{ANT_sac_pulse} = 0.5$$

$$N_{ANT_sac_end} = \begin{cases} N_{AG_FIX}(\theta_{sac_end}), & \text{if muscle became agonist after saccade} \\ N_{ANT_FIX}(\theta_{sac_end}), & \text{if muscle became antagonist after saccade} \end{cases}$$

The values for $N_{AG_sac_pulse}$ and $N_{ANT_sac_pulse}$ were selected by Bahill empirically (Bahill, Development, validation and sensitivity analyses of human eye movement models, 1980).

Fig. 8 presents the example of a neuronal control signal for the agonist muscle for a saccade with an amplitude of 30° , originating at the primary eye position 0° .

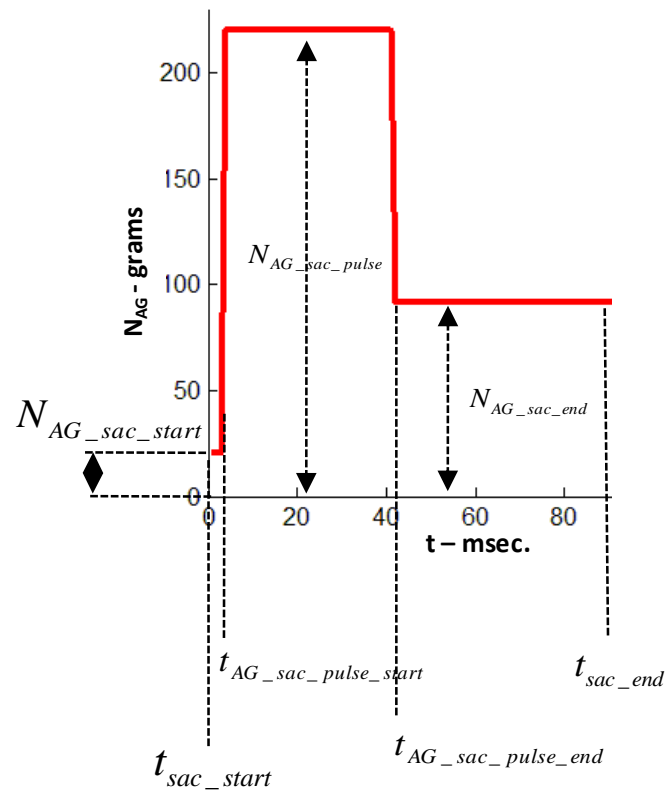


Fig. 8. Neuronal control signal N_{AG} for the agonist muscle for a saccade with a 30° amplitude.

3.3.8 Active State Tension

Though the neuronal control signal $N_{AG_sac}(t)$ and $N_{ANT_sac}(t)$, rises and drops instantaneously, neither the forces that muscles apply to the eye globe nor active state tensions rise to their maximum values immediately. This happens due to the anatomical characteristics of the neuronal signaling. A neuronal control signal spreading in a body is limited by: synchronization variations, synaptic transmission delays, motoneuronal firing frequency acceleration, neuronal conduction velocity, depolarization, spread of activity in the sarcoplasmic reticular formation. The rate of the neuronal control signal is affected by: synaptic transmissions, release and reuptake of the Ca^{++} , modification of the actin-myosin fibers (Bahill, Development, validation and sensitivity analyses of human eye movement models, 1980). In the proposed Mechanical Muscle Model, the active state tension is a result of a low pass filtering process performed upon the neuronal control signal.

The active state tension of the agonist and the antagonist muscles can be modeled by the following equations:

$$\hat{F}_{AG} = \begin{cases} N_{AG_sac_start}, t_{sac_start} \leq t < t_{AG_sac_pulse_start} & (19) \\ N_{AG_sac_start} \cdot e^{-\frac{t_{AG_sac_start}-t}{\tau_{AG_sac}}} + N_{AG_sac_pulse} \cdot \left(1 - e^{-\frac{t_{AG_sac_start}-t}{\tau_{AG_sac}}}\right), t_{AG_sac_pulse_start} \leq t < t_{AG_sac_pulse_end} \\ N_{AG_sac_pulse} \cdot e^{-\frac{t_{AG_sac_start}+t_{AG_sac_pulse}-t}{\tau_{AG_sac}}} + N_{AG_sac_end} \cdot \left(1 - e^{-\frac{t_{AG_sac_start}+t_{AG_sac_pulse}-t}{\tau_{AG_sac}}}\right), t_{AG_sac_pulse_end} \leq t < t_{sac_end} \end{cases}$$

$$\hat{F}_{ANT} = \begin{cases} N_{ANT_sac_start}, t_{sac_start} \leq t < t_{ANT_sac_pulse_start} & (20) \\ N_{ANT_sac_start} \cdot e^{-\frac{t_{ANT_sac_start}-t}{\tau_{ANT_sac}}} + N_{ANT_sac_pulse} \cdot \left(1 - e^{-\frac{t_{ANT_sac_start}-t}{\tau_{ANT_sac}}}\right), t_{ANT_sac_pulse_start} \leq t < t_{ANT_sac_pulse_end} \\ N_{ANT_sac_pulse} \cdot e^{-\frac{t_{ANT_sac_start}+t_{ANT_sac_pulse}-t}{\tau_{ANT_sac}}} + N_{ANT_sac_end} \cdot \left(1 - e^{-\frac{t_{ANT_sac_start}+t_{ANT_sac_pulse}-t}{\tau_{ANT_sac}}}\right), t_{ANT_sac_pulse_end} \leq t < t_{sac_end} \end{cases}$$

Fig. 9 represents an example of the active state tension developed inside the agonist muscle.

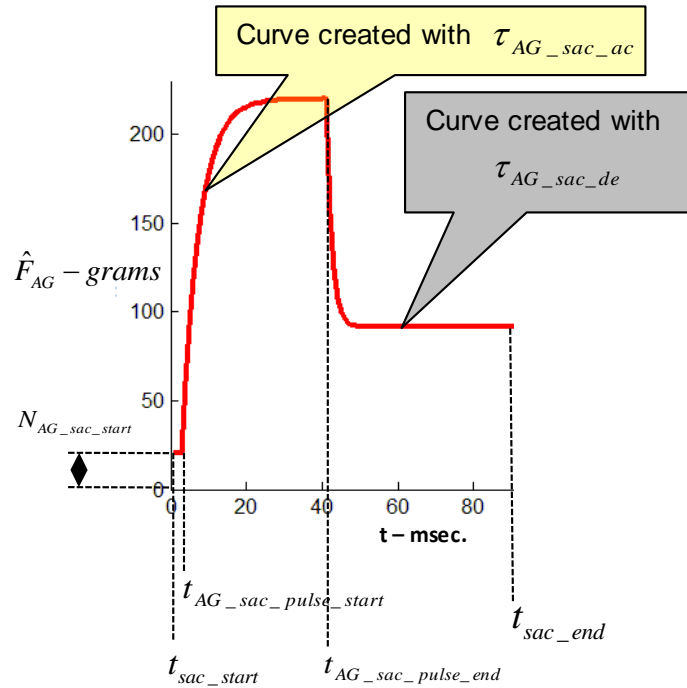


Fig. 9. Active state tension inside of the agonist muscle during a saccade originating at the primary position, with an amplitude of 30°.

The dynamics of the active state tension for the agonist muscle at every time interval

$[t_{sac_start}, t_{AG_sac_pulse_start})$,

$[t_{AG_sac_pulse_start}, t_{AG_sac_pulse_end})$, $[t_{AG_sac_pulse_end}, t_{sac_end})$ can be presented with

the following differential equation:

$$\dot{\hat{F}}_{AG}(t) = \frac{N_{AG} - \hat{F}_{AG}(t)}{\tau_{AG_sac}} \quad (21)$$

The dynamics of the active state tension for the antagonist muscle at every time

interval

$[t_{sac_start}, t_{ANT_sac_pulse_start})$,

$[t_{ANT_sac_pulse_start}, t_{ANT_sac_pulse_end})$, $[t_{ANT_sac_pulse_end}, t_{sac_end})$ can be presented

with this similar differential equation:

$$\dot{\hat{F}}_{ANT}(t) = \frac{N_{ANT} - \hat{F}_{ANT}(t)}{\tau_{ANT_sac}} \quad (22)$$

τ_{AG_sac} and τ_{ANT_sac} are functions that define the low pass filtering process; they are defined by the activation and deactivation time constants.

$$\tau_{AG_sac} = \begin{cases} \tau_{AG_sac_de}, & t_{sac_start} \leq t < t_{AG_sac_pulse_start} \\ \tau_{AG_sac_act}, & t_{AG_sac_pulse_start} \leq t < t_{AG_sac_pulse_end} \\ \tau_{AG_sac_de}, & t_{AG_sac_pulse_end} \leq t < t_{AG_sac_stop} \end{cases} \quad (23)$$

$$\tau_{ANT_sac} = \begin{cases} \tau_{ANT_sac_de}, & t_{sac_start} \leq t < t_{ANT_sac_pulse_start} \\ \tau_{ANT_sac_act}, & t_{ANT_sac_pulse_start} \leq t < t_{ANT_sac_pulse_end} \\ \tau_{ANT_sac_de}, & t_{ANT_sac_pulse_end} \leq t < t_{ANT_sac_stop} \end{cases} \quad (24)$$

Saccade activation time constants are:

$$\tau_{AG_sac_ac} = \begin{cases} 11.7 - 0.2 |\theta_{sac_amp}|, & \text{for } |\theta_{sac_amp}| \leq 50 \\ 13 - 0.1 |\theta_{sac_amp}|, & \text{for } |\theta_{sac_amp}| > 50 \end{cases}$$

$$\tau_{AG_sac_de} = 2$$

The value of $\tau_{AG_sac_de} = 0.2$ reported by Bahill in (Bahill, Development, validation and sensitivity analyses of human eye movement models, 1980) produces saccade

trajectories that do not correspond to human physiological data. Unfortunately several researchers who used Bahill's model in their work employed the erroneous value. Backtracking finds the value of $\tau_{AG_sac_de} = 2$ in (Hsu, Bahill, & Stark, 1976) that produces correct saccades.

Saccade deactivation time constants are:

$$\tau_{ANT_sac_ac} = 2.4$$

$$\tau_{ANT_sac_de} = 1.9$$

All presented activation/deactivation time constants are selected empirically to match human physiological data.

3.3.9 Oculomotor Plant Mechanical Model Equations

Positive amplitude saccades:

Saccades of positive amplitude are performed by the lateral rectus as the agonist and the medial rectus as the antagonist.

The diagram accounting for all forces inside of the horizontal OPMM during a positive amplitude saccade is presented in Fig. 10.

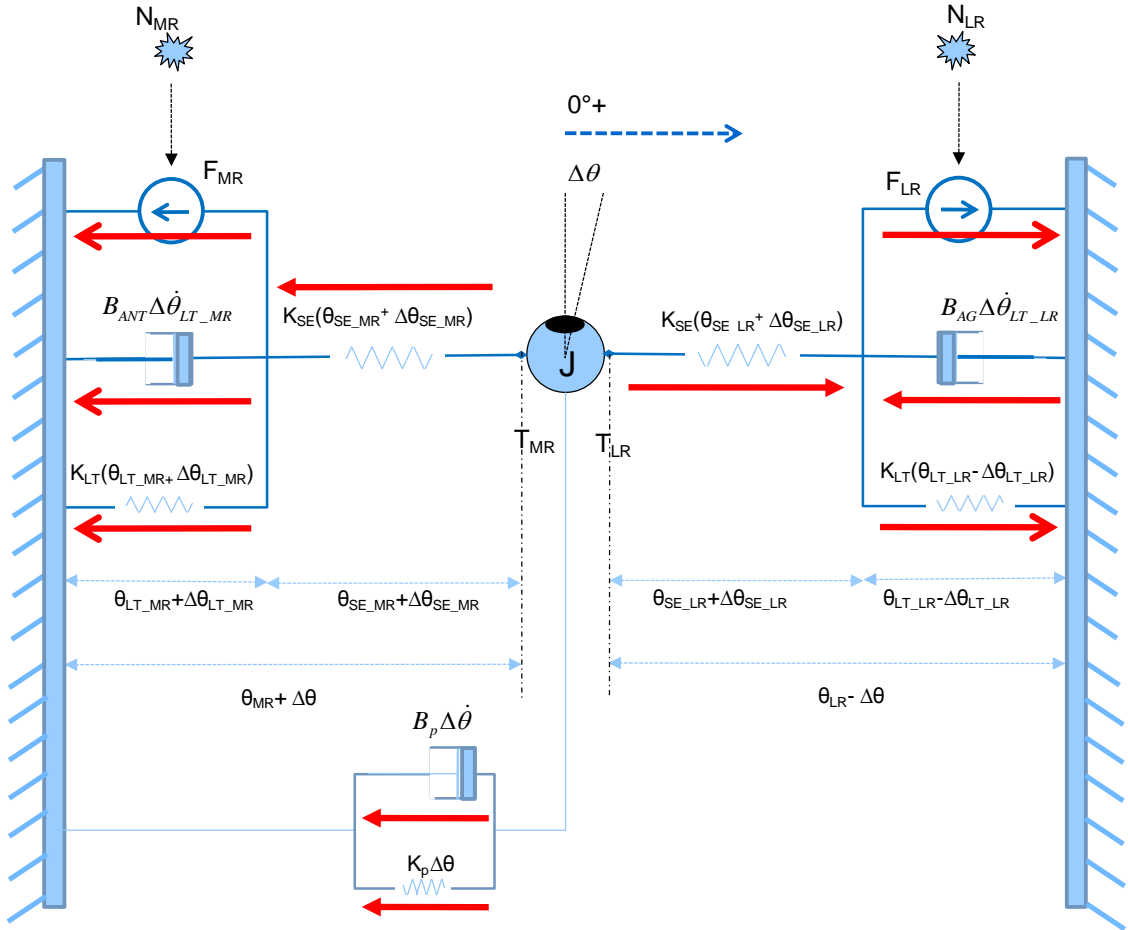


Fig. 10. The Oculomotor Plant Mechanical Model generating positive amplitude saccades. Arrows show the direction of forces for each component. F_{LR} , F_{MR} – active state tension; K_{LT} – length tension coefficient; K_{SE} – series elasticity coefficient; $\theta_{SE_MR} + \Delta\theta_{SE_MR}$, $\theta_{SE_LR} + \Delta\theta_{SE_LR}$ – length of the displacement of the series elasticity component of each muscle; $\theta_{LT_MR} + \Delta\theta_{LT_MR}$, $\theta_{LT_LR} - \Delta\theta_{LT_LR}$ – length of the displacement of the length tension component of each muscle; $\Delta\dot{\theta}_{LT_LR}$, $\Delta\dot{\theta}_{LT_MR}$ – velocity of change of the length tension component of the lateral and the medial recti; B_{AG} , B_{ANT} – damping coefficients for the agonist (the lateral rectus) and the antagonist (the medial rectus), $\Delta\theta$ – eye rotation; K_p – combined passive elasticity coefficient of the eye-orbit, both muscles and surrounding tissues; B_p – damping component coefficient for the viscosity of the eye-orbit and surrounding tissues. J is the rotational inertia of the eye globe.

The lateral rectus as the agonist applies the force to the eye globe that can be calculated by Equations 3 and 4. Those equations can be combined together:

$$K_{SE}(\Delta\theta_{LT_LR} - \Delta\theta) = \frac{K_{SE}\hat{F}_{LR}}{K_{SE} + K_{LT}} - \frac{\Delta\theta K_{SE}K_{LT}}{K_{SE} + K_{LT}} - \hat{B}_{AG}\Delta\dot{\theta}_{LT_LR} \quad (25)$$

The medial rectus as the antagonist applies the force to the eye globe that can be calculated by Equations 7 and 8. Those equations can be combined together:

$$K_{SE}(\Delta\theta - \Delta\theta_{LT_MR}) = \frac{K_{SE}\hat{F}_{MR}}{K_{SE} + K_{LT}} + \frac{\Delta\theta K_{SE}K_{LT}}{K_{SE} + K_{LT}} + \hat{B}_{ANT}\Delta\dot{\theta}_{LT_MR} \quad (26)$$

Applying Newton's second law, the sum of all forces acting on the eye globe equals the acceleration of the eye globe multiplied by the inertia of the eye globe.

$$J\Delta\ddot{\theta} = T_{LR} - T_{MR} - K_p\Delta\theta - B_p\Delta\dot{\theta} \quad (27)$$

J - eye globe's inertia, $\Delta\theta$ - eye rotation, $\Delta\dot{\theta}$ velocity of the eye rotation, $\Delta\ddot{\theta}$ eye rotation acceleration. T_{LR} can be calculated by Equation 4 and T_{MR} can be calculated by Equation 8. Thus Equation 27 can be transformed into:

$$J\Delta\ddot{\theta} = K_{SE}(\Delta\theta_{LT_LR} - \Delta\theta) - K_{SE}(\Delta\theta - \Delta\theta_{LT_MR}) - K_p\Delta\theta - B_p\Delta\dot{\theta} \quad (28)$$

There are five differential Equations - 21, 22, 25, 26, 28 - with six variables ($\Delta\theta$, $\Delta\theta_{LT_LR}$, $\Delta\theta_{LT_MR}$, $\Delta\dot{\theta}$, \hat{F}_{LR} , \hat{F}_{MR}) describing the eye movement during a positive amplitude saccade. A sixth differential equation can be added as:

$$\Delta\dot{\theta} = \Delta\dot{\theta} \quad (29)$$

Negative amplitude saccades:

Saccades of negative amplitude are performed by the medial rectus as the agonist

and the lateral rectus as the antagonist.

The following equations describe the muscle movement dynamics during saccades of the negative amplitude:

$$K_{SE}(\Delta\theta_{LT_LR} - \Delta\theta) = \frac{\hat{F}_{LR}K_{SE}}{K_{SE} + K_{LT}} - \frac{\Delta\theta K_{SE}K_{LT}}{K_{SE} + K_{LT}} - \hat{B}_{ANT}\Delta\dot{\theta}_{LT_LR} \quad (30)$$

$$K_{SE}(\Delta\theta - \Delta\theta_{LT_MR}) = \frac{\hat{F}_{MR}K_{SE}}{K_{SE} + K_{LT}} + \frac{\Delta\theta K_{SE}K_{LT}}{K_{SE} + K_{LT}} + \hat{B}_{AG}\Delta\dot{\theta}_{LT_MR} \quad (31)$$

$$J\Delta\ddot{\theta} = K_{SE}(\Delta\theta_{LT_LR} - \Delta\theta) - K_{SE}(\Delta\theta - \Delta\theta_{LT_MR}) + K_p\Delta\theta + B_p\Delta\dot{\theta} \quad (32)$$

Appendix A.3 presents the details of deriving Equations 30-32.

There are five differential Equations - 21, 22, 30, 31, 32 - with six variables ($\Delta\theta$, $\Delta\theta_{LT_LR}$, $\Delta\theta_{LT_MR}$, $\Delta\dot{\theta}$, \hat{F}_{LR} , \hat{F}_{MR}) describing the eye movement during a positive amplitude saccade. A sixth differential equation can be added as:

$$\Delta\dot{\theta} = \Delta\dot{\theta} \quad (33)$$

It is remarkable to note that Equation 30, representing the force dynamics of the lateral rectus, is almost the same as Equation 25, except the value of the dashpot coefficient. The same fact can be noted about the Equation 31 and Equation 26. This result indicates that the mechanical dynamics remain essentially the same for each muscle independent of the role this muscle plays during a saccade.

The equation mapping all forces acting on the eye globe to the eye acceleration and inertia during a saccade is the same for the saccades of both negative and positive amplitudes.

3.3.10 Example

Fig. 11 represents an example of the force applied by the lateral rectus to the eye globe $K_{SE}(\theta_{LT_LR} - \theta)$ and force applied by the medial rectus to the eye globe $K_{SE}(\theta - \theta_{LT_MR})$ during a saccade with an amplitude of -25° starting from -5° from the primary eye position.

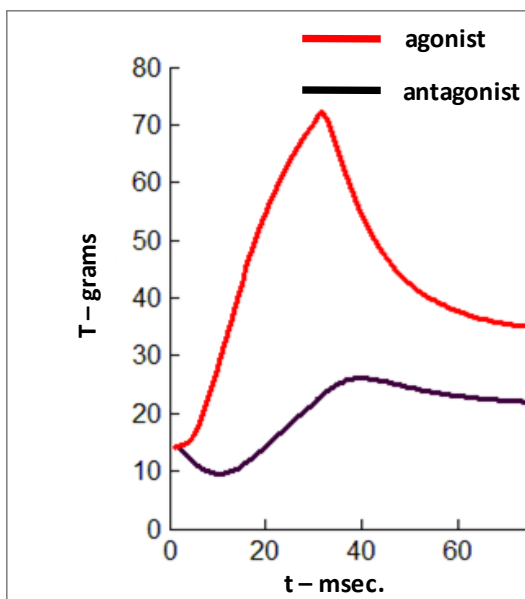


Fig. 11. Force applied by the lateral and the medial recti to the eye globe during a saccade of -25° , originating at -5° of the primary eye position.

The Oculomotor Plant Mechanical Model was presented in this Chapter. Neuronal control and mechanical modeling of eye characteristics were discussed.

CHAPTER 4

Oculomotor Plant Kalman Filter Framework

The Kalman Filter is the backbone of the framework developed in this Dissertation. The Kalman Filter is responsible for the continuous prediction of the eye movement signal. The challenge of combining a mechanical model of the eye and a Kalman Filter lies in the transformation of the eye model into a form that conforms to the process transition mechanics employed by the Kalman Filter. The main challenges of such a transformation are: prediction of eye movement trajectories during various eye movement types, defining transition mechanics for “left” and “right” saccades, determining measurement noise parameters and mechanical model noise parameters. The details of the transformation are presented in this Chapter.

4.1 Basics of Kalman Filtering

The Kalman filter is a recursive estimator that computes a future estimate of the dynamic system state from a series of incomplete and noisy measurements. A Kalman Filter minimizes the error, between the estimation of the system’s state and the actual system’s state. Only the estimated state from the previous time step and the new measurements are needed to compute the new state estimate. Many real dynamic

systems do not exactly fit this model; however, because the Kalman filter is designed to operate in the presence of noise, an approximate fit is often adequate for the filter to be very useful (Brown & Hwang, 1997).

The Kalman Filter addresses the problem of trying to estimate the state $x \in \mathfrak{R}^n$ of a discrete-time controlled process that is governed by the linear stochastic difference equation (Brown & Hwang, 1997):

$$x_{k+1} = A_{k+1}x_k + B_{k+1}u_{k+1} + w_{k+1} \quad (34)$$

with the measurement

$$z_k = H_k x_k + v_k \quad (35)$$

The n-by-n state transition matrix A_{k+1} relates the state at the previous time step k to the state at the current step k+1, in the absence of either a driving function or process noise. B_{k+1} is an n-by-m control input matrix, that relates m-by-1 control vector u_{k+1} to the state x_k . w_k is an n-by-1 process noise vector with an n-by-n covariance matrix Q_k . $p(w_k) \sim N(0, Q_k)$. Not all variables in the state are visible to the measuring instruments. The measurement vector z_k contains state variables that are measured by the instruments. H_k is a j-by-n observation model matrix which maps the state x_k into the measurement vector z_k . v_k is a measurement noise j-by-1 vector with covariance R_k . $p(v_k) \sim N(0, R_k)$.

The Discrete Kalman filter has two distinct phases that compute the estimate of the next system's state (Brown & Hwang, 1997).

Predict:

Predict the state vector ahead:

$$\hat{x}_{k+1}^- = A_{k+1}x_k + B_{k+1}u_{k+1} \quad (36)$$

The \hat{x}_{k+1}^- is used as the future eye position coordinate for predicting eye movement trajectories.

Predict the error covariance matrix ahead:

$$P_{k+1}^- = A_{k+1}P_kA_{k+1}^T + Q_{k+1} \quad (37)$$

The predict phase uses the previous state estimate to predict the estimate of the next system's state.

Update:

Compute the Kalman gain:

$$K_{k+1} = P_{k+1}^- H_{k+1}^T (H_{k+1} P_{k+1}^- H_{k+1}^T + R_{k+1})^{-1} \quad (38)$$

Update the estimate of the state vector with a measurement z_{k+1} :

$$\hat{x}_{k+1} = \hat{x}_{k+1}^- + K_{k+1}(z_{k+1} - H_{k+1}\hat{x}_{k+1}^-) \quad (39)$$

Update the error covariance matrix:

$$P_{k+1} = (I - K_{k+1}H_{k+1})P_{k+1}^- \quad (40)$$

It should be pointed out that the Kalman Filter maintains first two moments of the state distribution $E[x_k] = \hat{x}_k$, $E[(x_k - \hat{x}_k)(x_k - \hat{x}_k)^T] = P_k$ and $p(x_k | z_k) \sim N(E[x_k], E[(x_k - \hat{x}_k)(x_k - \hat{x}_k)^T]) = N(\hat{x}_k, P_k)$. The choice of the Kalman gain K_k minimizes error covariance matrix P_k .

Kalman Filter framework assumes that x_k, z_k are normally distributed and $E[v_k v_i^T] =$

$$\begin{cases} R_k & i = k \\ 0 & i \neq k \end{cases}, \quad E[w_k, w_i^T] = \begin{cases} Q_k & i = k \\ 0 & i \neq k \end{cases}, \quad E[w_k e_i^T] = 0 \quad \forall i, k. \quad [41].$$

4.2 Oculomotor Plant Kalman Filter Design

This section presents the Oculomotor Plant Kalman Filter (OPKF) framework for horizontal eye movements. Current implementation of the OPKF framework predicts an eye movement trajectory by the Two State Kalman Filter (TSKF) during all eye movements except saccades. The TSKF detects the onset of saccades by the mechanism described in Section 5.2. During saccades the OPMM integrated into the Kalman Filter predicts the eye movement trajectory.

The challenge of designing the OPKF lies in the transformation of the OPMM into the form that conforms to the process transition mechanics employed by the Kalman Filter. Specifically it is necessary to define a state vector x_k , control vector u_k , transition matrix A_k , control matrix B_k . It is also necessary to derive a covariance matrix Q_k for the system's noise w_k and covariance matrix R_k defining measurement noise v_k . Additionally to map actual system's state vector x_k to the measurement vector z_k represented by Equation 35 observation matrix H_k is required.

State vector: x_k

Following values are selected to represent the state vector:

$$x_k = [x_1(k) \quad x_2(k) \quad x_3(k) \quad x_4(k) \quad x_5(k) \quad x_6(k)]^T \quad (41)$$

$x_1(k) = \Delta\theta$ – eye rotation, $x_2(k) = \Delta\theta_{LT_LR}$ – displacement of the length tension

component for the lateral rectus as a result of $\Delta\theta$ rotation, $x_3(k) = \Delta\theta_{LT_MR}$ -

displacement of the length tension component for the medial rectus as a result of $\Delta\theta$

rotation, $x_4(k) = \Delta\dot{\theta}$ – eye velocity, $x_5(k) = \hat{F}_{LR}$ – the lateral rectus active state tension, $x_6(k) = \hat{F}_{MR}$ – the medial rectus active state tension.

Transition matrix, control matrix, control vector: A_k, B_k, u_k .

The transition matrix required for Equation 36 will be defined for two eye movement groups. Group 1 will consists of eye fixations and smooth pursuits. Group 2 will consist of saccades. The eye movement trajectory will be predicted by the TSKF during eye movements representing the Group 1 and the OPMM integrated into the Kalman Filter will be used for prediction during eye movements representing Group 2. It should be mentioned that all saccades will be divided into the positive and negative amplitude saccades. Positive amplitude saccades will require a different transition matrix A_k then the negative amplitude saccades.

Two State Kalman Filter

The Two State Kalman Filter (TSKF) uses only eye position $\Delta\theta$ and eye velocity $\Delta\dot{\theta}$ parameters for the eye movement prediction. Knowing that $x_1(k) = \Delta\theta$ and $x_4(k) = \Delta\dot{\theta}$, the horizontal eye movement dynamics can be represented by a differential equation $\dot{x}_1(k) = x_4(k)$. Approximating derivative as $\dot{x}(k) = \frac{x(k+1)-x(k)}{\Delta t}$ the equation $\dot{x}_1(k) = x_4(k)$ can be rewritten as:

$$x_1(k+1) = x_1(k) + x_4(k)\Delta t \quad (42)$$

It is possible to re-write Equation 42 in the following matrix form:

$$x_{k+1} = A_{k+1}x_k + B_{k+1}u_{k+1} \quad (43)$$

where x_k, x_{k+1} are state vectors defined by Equation 41 and A_{k+1} is a transition matrix:

$$A_{k+1} = \begin{pmatrix} 1 & 0 & 0 & \Delta t & 0 & 0 \\ 0 & 0 & 0 & 0 & 0 & 0 \\ 0 & 0 & 0 & 0 & 0 & 0 \\ 0 & 0 & 0 & 1 & 0 & 0 \\ 0 & 0 & 0 & 0 & 0 & 0 \\ 0 & 0 & 0 & 0 & 0 & 0 \end{pmatrix} \quad (44)$$

where Δt is eye tracker's eye position sampling interval.

Control matrix B_{k+1} and control vector u_{k+1} are zero for the TSKF.

The TSKF is capable of detecting saccades using mechanism described in Section 5.2.

Once a saccade is detected and the amplitude and the direction of the saccade is determined, differential equations defining the OPMM are used to create the transition matrix A_{k+1} , control matrix B_{k+1} and control vector u_{k+1} . This calculation is done using the approximate definition of derivative as $\dot{x}(k) = \frac{x(k+1)-x(k)}{\Delta\rho}$ where $\Delta\rho$ is the OPMM internal sampling clock¹.

Positive amplitude saccades:

Differential Equations 29, 25, 26, 28, 21, 22 are used to derive A_k , B_k , u_k for the OPKF framework during saccades of the positive amplitude.

First those equations are transformed into the following form:

$$\dot{x}_1(t) = x_4(t) \quad (45)$$

¹ The Oculomotor Plant Mechanical Model generates best results with internal clock $\Delta\rho=0.001$ sec. due to neuronal control signal changing on the millisecond level. If the internal clock is larger than 1 msec. the difference between the actual eye movement trajectory and the trajectory generated by oculomotor plant mechanical model will increase.

$$\dot{x}_2(t) = \frac{K_{SE}^2}{(K_{LT} + K_{SE})\hat{B}_{AG}} x_1(t) - \frac{K_{SE}}{\hat{B}_{AG}} x_2(t) + \frac{K_{SE}}{(K_{LT} + K_{SE})\hat{B}_{AG}} x_5(t) \quad (46)$$

$$\dot{x}_3(t) = \frac{K_{SE}^2}{(K_{LT} + K_{SE})\hat{B}_{ANT}} x_1(t) - \frac{K_{SE}}{\hat{B}_{ANT}} x_3(t) - \frac{K_{SE}}{(K_{LT} + K_{SE})\hat{B}_{ANT}} x_6(t) \quad (47)$$

$$\dot{x}_4(t) = -\frac{2K_{SE} + K_p}{J} x_1(t) + \frac{K_{SE}}{J} x_2(t) + \frac{K_{SE}}{J} x_3(t) - \frac{B_p}{J} x_4(t) \quad (48)$$

$$\dot{x}_5(t) = \frac{N_{LR} - x_5(t)}{\tau_{AG}} \quad (49)$$

$$\dot{x}_6(t) = \frac{N_{MR} - x_6(t)}{\tau_{ANT}} \quad (50)$$

Second the transition matrix A_k , control matrix B_k , control vector u_k are calculated.

$$A_k = \begin{pmatrix} 1 & 0 & 0 & \Delta\rho & 0 & 0 \\ \Delta\rho \frac{K_{SE}^2}{(K_{LT} + K_{SE})\hat{B}_{AG}} & \left(1 - \Delta\rho \frac{K_{SE}}{\hat{B}_{AG}}\right) & 0 & 0 & \Delta\rho \frac{K_{SE}}{(K_{LT} + K_{SE})\hat{B}_{AG}} & 0 \\ \Delta\rho \frac{K_{SE}^2}{(K_{LT} + K_{SE})\hat{B}_{ANT}} & 0 & \left(1 - \Delta\rho \frac{K_{SE}}{\hat{B}_{ANT}}\right) & 0 & 0 & -\Delta\rho \frac{K_{SE}}{(K_{LT} + K_{SE})\hat{B}_{ANT}} \\ -\Delta\rho \frac{2K_{SE} + K_p}{J} & \Delta\rho \frac{K_{SE}}{J} & \Delta\rho \frac{K_{SE}}{J} & 1 - \Delta\rho \frac{B_p}{J} & 0 & 0 \\ 0 & 0 & 0 & 0 & \left(1 - \frac{\Delta\rho}{\tau_{AG}}\right) & 0 \\ 0 & 0 & 0 & 0 & 0 & \left(1 - \frac{\Delta\rho}{\tau_{ANT}}\right) \end{pmatrix} \quad (51)$$

$$u_k = \left[0 \quad 0 \quad 0 \quad 0 \quad \frac{\Delta\rho}{\tau_{AG}} N_{LR} \quad \frac{\Delta\rho}{\tau_{ANT}} N_{MR} \right]^T \quad (52)$$

The control matrix B_k is a 6x6 identity matrix.

Calculations are done in the detail in Appendix A.4, here only the final result is presented.

Negative amplitude saccades:

Differential Equations 33, 30, 31, 32, 22, 21 are used to derive A_k , B_k , u_k for the

OPKF framework during saccades of the negative amplitude.

$$\dot{x}_1(t) = x_4(t) \quad (53)$$

$$\dot{x}_2(t) = \frac{K_{SE}^2}{(K_{LT} + K_{SE})\hat{B}_{ANT}} x_1(t) - \frac{K_{SE}}{\hat{B}_{ANT}} x_2(t) + \frac{K_{SE}}{(K_{LT} + K_{SE})\hat{B}_{ANT}} x_5(t) \quad (54)$$

$$\dot{x}_3(t) = \frac{K_{SE}^2}{(K_{LT} + K_{SE})\hat{B}_{AG}} x_1(t) - \frac{K_{SE}}{\hat{B}_{AG}} x_3(t) - \frac{K_{SE}}{(K_{LT} + K_{SE})\hat{B}_{AG}} x_6(t) \quad (55)$$

$$\dot{x}_4(t) = -\frac{2K_{SE} + K_p}{J} x_1(t) + \frac{K_{SE}}{J} x_2(t) + \frac{K_{SE}}{J} x_3(t) - \frac{B_p}{J} x_4(t) \quad (56)$$

$$\dot{x}_5(t) = \frac{N_{LR} - x_5(t)}{\tau_{ANT}} \quad (57)$$

$$\dot{x}_6(t) = \frac{N_{MR} - x_6(t)}{\tau_{AG}} \quad (58)$$

Second the transition matrix A_k , control matrix B_k , control vector u_k are calculated.

$$A_k = \begin{pmatrix} 1 & 0 & 0 & \Delta\rho & 0 & 0 \\ \Delta\rho \frac{K_{SE}^2}{\hat{B}_{AG}(K_{LT} + K_{SE})} \left(1 - \Delta\rho \frac{K_{SE}}{\hat{B}_{AG}}\right) & 0 & 0 & 0 & \Delta\rho \frac{K_{SE}}{\hat{B}_{ANT}(K_{LT} + K_{SE})} & 0 \\ \Delta\rho \frac{K_{SE}^2}{\hat{B}_{ANT}(K_{LT} + K_{SE})} & 0 & \left(1 - \Delta\rho \frac{K_{SE}}{\hat{B}_{ANT}}\right) & 0 & 0 & -\Delta\rho \frac{K_{SE}}{\hat{B}_{AG}(K_{LT} + K_{SE})} \\ \Delta\rho \frac{2K_{SE} + K_p}{J} & \Delta\rho \frac{K_{SE}}{J} & \Delta\rho \frac{K_{SE}}{J} & 1 - \Delta\rho \frac{B_p}{J} & 0 & 0 \\ 0 & 0 & 0 & 0 & \left(1 - \frac{\Delta\rho}{\tau_{ANT}}\right) & 0 \\ 0 & 0 & 0 & 0 & 0 & \left(1 - \frac{\Delta\rho}{\tau_{AG}}\right) \end{pmatrix} \quad (59)$$

$$u_k = \left[0 \quad 0 \quad 0 \quad 0 \quad \frac{\Delta\rho}{\tau_{ANT}} N_{LR} \quad \frac{\Delta\rho}{\tau_{AG}} N_{MR} \right]^T \quad (60)$$

The control matrix B_k is a 6x6 identity matrix.

Calculations are similar to those presented in the Appendix A.4, here only the final result is presented.

Measurement vector, observation matrix: z_k, H_k .

The eye position measurement device is an eye tracker. An eye tracker reports horizontal and vertical eye position coordinates with a time stamp. In this Dissertation only horizontal component of the recorded eye movements is considered, thus measurement vector z_k is a scalar that represents horizontal eye coordinate recorded by the eye tracker at the time k .

The OPMM has six states, but only the eye position is observed, thus observation matrix has the following form:

$$H_k = [1 \quad 0 \quad 0 \quad 0 \quad 0 \quad 0] \quad (61)$$

Measurement noise covariance matrix, system's noise covariance matrix: R_k, Q_k .

By definition the covariance matrix for the measurement noise is $R_k = E[(v_k - E(v_k))(v_k - E(v_k))^T]$. Because only eye position is measured v_k is a scalar making $R_k = VAR[v_k] = \delta_v^2$, where δ_v is the standard deviation of the measurement noise. In this Dissertation it is assumed that the standard deviation of the measurement noise relates to the accuracy of the eye tracker and is bounded by one degree of the visual angle. This logic is used to select $\delta_v = 1^\circ$.

$$R_k = \delta_v^2 = 1 \quad (62)$$

In case when the eye tracker fails to detect eye position coordinates the standard deviation of measurement noise is assigned to be $\delta_v = 120^\circ$. The value of 120° is chosen empirically, allowing Kalman Filter to “trust” more predicted eye position

coordinate \hat{x}_k^- .

$$R_k = \delta_v^2 = 120^2 \quad (63)$$

The eye tracker that was used in this Dissertation has the eye position sampling clock (50Hz), which is much slower than the OPMM internal clock (1000Hz). In cases when the OPMM makes the estimate of the current eye position but the measurement from the eye tracker is not available the measurement noise covariance matrix represented by Equation 63 is used and the last observed eye position coordinate is assigned to the measurement z_k . Such large standard deviation value allows Kalman Filter to rely on the prediction estimate calculated by Equation 36.

By definition system's noise covariance matrix is $Q_k = E[(w_k - E(w_k))(w_k - E(w_k))^T]$, where w_k is a 1x6 system's noise vector $w_k = [w_1(k) \ w_2(k) \ w_3(k) \ w_4(k) \ w_5(k) \ w_6(k)]^T$. In this Dissertation it is assumed that variables $w_i(k)$ are uncorrelated between each other i.e. $E[(w_m(k)w_n(k))] = E[(w_m(k))E[w_n(k)]]$ for all $n \neq m$.

This assumption generates following system's noise covariance matrix:

$$Q_k = \begin{bmatrix} \delta_1^2 & \dots & 0 \\ \dots & \dots & \dots \\ 0 & \dots & \delta_6^2 \end{bmatrix} \quad (64)$$

Here $\delta_1^2, \dots, \delta_6^2$ are variances of variables $w_i(k)$. In this Dissertation it is assumed that the standard deviation of the eye position noise $w_1(k)$ is connected to the characteristics of the eye fixation movement. This is done with the assumption that eye fixation is the most common type of the eye movement. Each eye fixation consists of

three basic eye-sub-movements: drift, small involuntary saccades and tremor (Yarbus, 1967). Among those three, involuntary saccades have the highest amplitude - around half degree of the visual angle. 1° is selected as the upper movement boundary, making $\delta_1 = 1^\circ$. Standard deviation values for other variables are hard to assess, but the following values performed well in the simulation tests: $\delta_2 = \delta_3 = 1^\circ$ degree, $\delta_4 = 1^\circ/\text{sec.}$, $\delta_5 = \delta_6 = 1$ gram.

Initial values for state vector and error covariance matrices: x_0, P_0 .

It is important to underline that the OPKF framework uses different initial values for the state vector belonging to Group 1 (fixations, pursuits) and Group 2 (saccades).

Group 1

Initial state vector is $x_0 = [x_1(0) \ x_2(0) \ x_3(0) \ x_4(0) \ x_5(0) \ x_6(0)]^T$ Here last measured horizontal eye position coordinate² is assigned to $x_1(0)$ and $x_2(0) = x_3(0) = x_4(0) = x_5(0) = x_6(0) = 0$.

Group 2

The initial values for the system's state vector for each saccade are: $x_1(0)$ - horizontal saccade onset eye position; $x_2(0) = x_1(0) + 5.6^\circ$ - initial displacement of the length of the lateral rectus length tension component; $x_3(0) = x_1(0) - 5.6^\circ$ - initial displacement of the length of the medial rectus length tension component; $x_4(0) = 0$ -

² In case when the horizontal eye position coordinate is not available the coordinate of the screen center is used.

initial value of the eye velocity; initial active state tension for the lateral rectus is calculated using Equations 11 and 12 in the following form

$$x_5(0) = \begin{cases} N_{AG_FIX}(x_1(0)) & \text{if lateral rectus was agonist prior to saccade} \\ N_{ANT_FIX}(x_1(0)) & \text{if lateral rectus was antagonist prior to saccade} \end{cases} ;$$

initial active state tension for the medial rectus is calculated following the same logic

$$x_6(0) = \begin{cases} N_{AG_FIX}(x_1(0)) & \text{if medial rectus was agonist prior to saccade} \\ N_{ANT_FIX}(x_1(0)) & \text{if medialrectus was antagonist prior to saccade} \end{cases} .$$

The initial error covariance matrix P_0 is a 6x6 identity matrix for both groups of the eye movements.

A transformation of the Oculomotor Plant Mechanical Model into a form that can be used by a Kalman Filter was presented in this Chapter.

CHAPTER 5

Detection of Basic Eye Movement Types

Eye movement type detection is the core issue in eye tracking. Each eye movement type has its own unique characteristics, and it is important to evaluate each eye movement prediction model for every eye movement type. This Chapter describes one of the most common eye movement detection methods called I-VT. This Dissertation uses the I-VT method as the main method for eye movement type classification. Saccade detection by a Kalman Filter is discussed in the second part of the Chapter as the method that has the capability of predicting future saccades amplitudes by analyzing a chi square test value.

5.1 Velocity-Threshold Identification (I-VT)

An IV-T is a velocity-based model that detects eye movement types based on their point to point velocities (Salvucci & Goldberg, Identifying fixations and saccades in eye tracking protocols, 2000). Eye fixation is detected when the eye speed does not exceed $20^{\circ}/\text{sec}$ and this velocity pattern lasts for at least 100 msec., which is considered to be the minimum duration interval for an eye fixation. A saccades is detected when the eye velocity exceeds $300^{\circ}/\text{sec}$. Saccade duration is calculated using

the formula presented by Carpenter (Carpenter, 1977)

$$D = 2.2 * \theta_{\text{sac_amp}} + 21 \quad (65)$$

where D is the duration of the saccade measured in msec. and $\theta_{\text{sac_amp}}$ is the amplitude of the saccade measured in degrees (Carpenter, 1977). Pursuits are detected when the eye velocity is in the 20-300°/sec range. An I-VT eye movement detection model has good real-time performance.

5.2 Saccade Detection by the Two State Kalman Filter

Saccade detection was performed through the method proposed by Sauter (Sauter, J., Di Renzo, & Vomscheid, 1991). The idea behind this method is to monitor the differences between the predicted eye-velocity and the observed eye-velocity. The predicted eye-velocity is calculated by the Two State Kalman Filter introduced in Section 4.2. The difference between the predicted eye velocity and the observed eye velocity is monitored by a chi square test:

$$\chi^2 = \sum_{i=1}^p \frac{\left(\hat{x}_4^-(i) - \left(\frac{z_i - z_{i-1}}{\Delta t} \right) \right)^2}{\delta^2} \quad (66)$$

where $\hat{x}_4^-(i)$ is the predicted eye velocity computed by Equation 36 and z_i is the measured eye position coordinate. Δt is the eye tracker's sampling interval. δ is the standard deviation of the observed eye velocity during the sampling interval under consideration. Once a specified threshold of the χ^2 is achieved a saccade is detected (value of $\chi^2 = 100$ is used in this Dissertation). It was reported by Grindiger

(Grinding, 2006) that the filter behaves better if the standard deviation δ is a constant. The experiments conducted in this Dissertation use values $\delta^2 = 1000$ and $p = 5$ proposed by Grinding (Grinding, 2006). The saccade detection performance achieved by the chi square test with these parameters is almost identical to the I-VT model. Saccade detection by the TSKF is real-time.

In previous work (Komogortsev & Khan, Kalman Filtering in the Design of Eye-Gaze-Guided Computer Interfaces, 2007) I have explored the possibility of designing a function that determines saccade amplitude based on the chi square value, however that function was not 100% accurate. This function had the following form:

$$A_{sac_amp} = -0.000024\chi^6 + 0.0536\chi^4 + 1.5 \quad (67)$$

In this Dissertation the Two State Kalman Filter detects the onset of a saccade, but the amplitude of a saccade is calculated as a difference between the eye position at the end of the saccade and the eye position at the beginning of the next saccade.

Two models of eye movement detection were presented in this Chapter. The first model was used to evaluate the accuracy of the eye movement prediction models created in this Dissertation.

CHAPTER 6

Methodology

This Chapter presents four eye movement prediction models. The properties of the environment used to test the models are described. The metric defining the accuracy of eye movement prediction is described.

6.1 Equipment

The proposed OPKF framework was tested with a Tobii 1750 Eye Tracker. The 1750 model has the following characteristics: accuracy - 0.5° , drift less than 0.5° , and eye position scanning frequency – 50Hz. The Tobii 1750 model provides binocular tracking and compensates for small head movements within a 30 x 16 x 20 cm window, thus it was not required to stabilize a subject's head. Nevertheless, during the experiments every subject was asked to hold his/her head motionless. Before running each experiment, the eye tracking equipment was calibrated for the subject and checked for calibration accuracy.

6.2 Test Media

Human eye movements are highly dependent upon the visual content. The pattern of the eye movement changes depends on the complexity of the scene. Unfortunately, there are no easy or agreed upon means of measuring such complexity. Several video clips were evaluated subjectively. Three video clips were selected to test the performance of the OPKF framework. Below are rough subjective-complexity descriptions for each video clip:

Car: This video shows a moving car. It was taken from a security camera view point in a university parking lot. The visible size of the car was approximately one fifth of the screen. The car was moving slowly, allowing the subject to develop smooth pursuit movements. Several pedestrians and distant cars appeared on the background several times, often capturing the attention of the subject. The remaining part of video's background was still. The snapshot is presented in Fig. 12.



Fig. 12. Car video snapshot.

Shamu: This video captures a night performance of Shamu at a Sea World, under a tracking spotlight. The video consists of several moving objects: Shamu, the trainer,

and the crowd. Each of those objects is moving at different speeds during various periods of time. The interesting aspect of this video is that a subject can concentrate on different objects and it would result in a variety of eye movements: fixations, saccades, and smooth pursuits. The background of the video was constantly in motion due to the fact that the camera was trying to follow the swimming Shamu. Such an environment suits the goal of challenging the OPKF to deal with different types of eye movements. The fact that the clip was taken during the night provides an interesting aspect of the video perception by a subject. The snapshot is presented in Fig. 13.



Fig. 13. Shamu video snapshot.

Airplanes: This video depicts formation flying of supersonic planes, rapidly changing their flying speeds. It was from a performance of the Blue Angels over Lake Erie in Cleveland. The number of planes varies from one to five during the clip. The scene-recording camera movements were rapid zoom and panning. Frequently the camera could not focus very well on a plane and the subject had to search for it. This aspect brought an additional complication to the general pattern of eye movements.

The background of this video was in constant motion and presented a blue sky. The snapshot is presented in Fig. 14.



Fig. 14. Airplanes video snapshot.

All three videos had a resolution of 720x480 pixels, presented with a frame-rate of 30fps, and were 1 minute long.

Subjectively it was possible to say that the “Car” video clip was the least challenging to the HVS. The “Shamu” video clip was more challenging than “Car”. The “Airplanes” video clip was the most challenging to the HVS.

6.3 Participants

The subject pool consisted of 21 volunteers of both genders and mixed ethnicities, aged 20-40 with normal, corrected and uncorrected vision. The subjects were instructed to watch the video clips in any way they wanted. The psychological literature classifies such a viewing setup as a bottom-up saliency viewing experiment.

6.4 Eye Movement Prediction Models

In this Subsection four distinct eye movement prediction models are presented. All four models consist of the components that define the OPKF framework.

6.4.1 Two State Kalman Filter (TSKF)

The design of the TSKF prediction model was described in Section 4.2. The TSKF uses only eye position $\Delta\theta$ and eye velocity $\Delta\dot{\theta}$ component to predict future eye movement. The TSKF model predicts eye movement trajectories during all types of eye movements.

The concept of eye movement prediction by the TSKF prediction model is diagrammatically represented in Fig. 15.

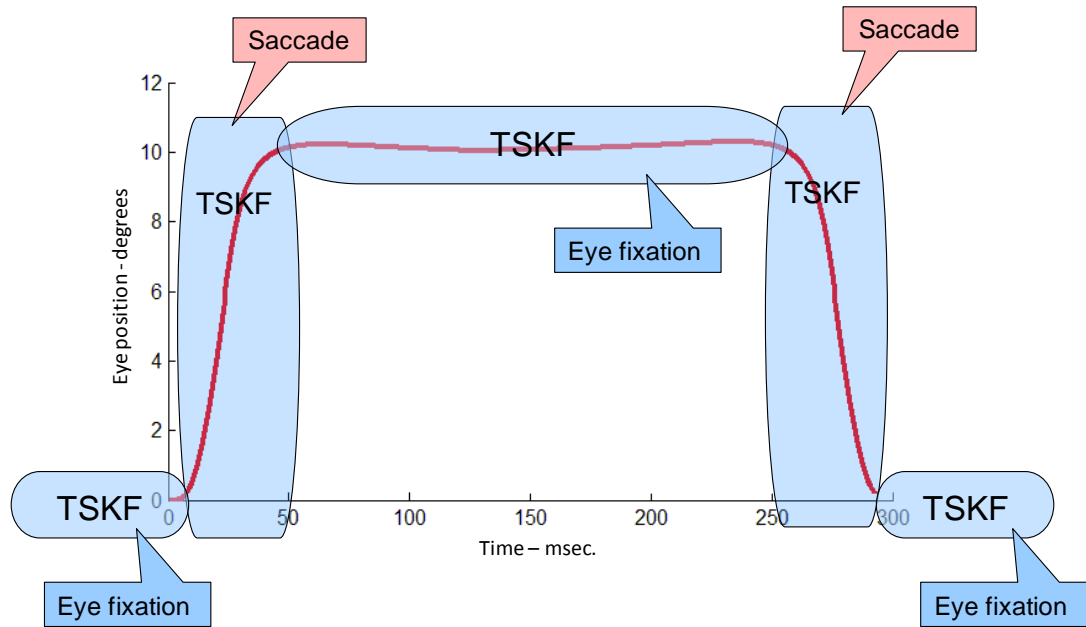


Fig. 15. Eye movement prediction by the TSKF model. The TSKF predicts eye movement trajectories during all eye movements.

6.4.2 Oculomotor Plant Mechanical Model (OPMM)

The OPMM eye movement prediction model uses the TSKF to predict eye movement trajectories during all eye movements except saccades. Once the TSKF detects a saccade the OPMM predicts the eye movement trajectory for the duration of the saccade. After the saccade ends the TSKF predicts the eye movement trajectory until the beginning of the next saccade.

The OPMM predicts eye movement trajectories during a saccade only by employing Equation 36.

$$\hat{x}_{k+1}^- = A_{k+1}x_k + B_{k+1}u_{k+1}$$

The OPMM does not use eye position measurements obtained by the eye tracker during saccades. The OPMM does not use process noise or measurement noise covariance matrixes employed by the “full” OPKF.

The concept of eye movement prediction by the OPMM prediction model is diagrammatically represented in Fig. 16.

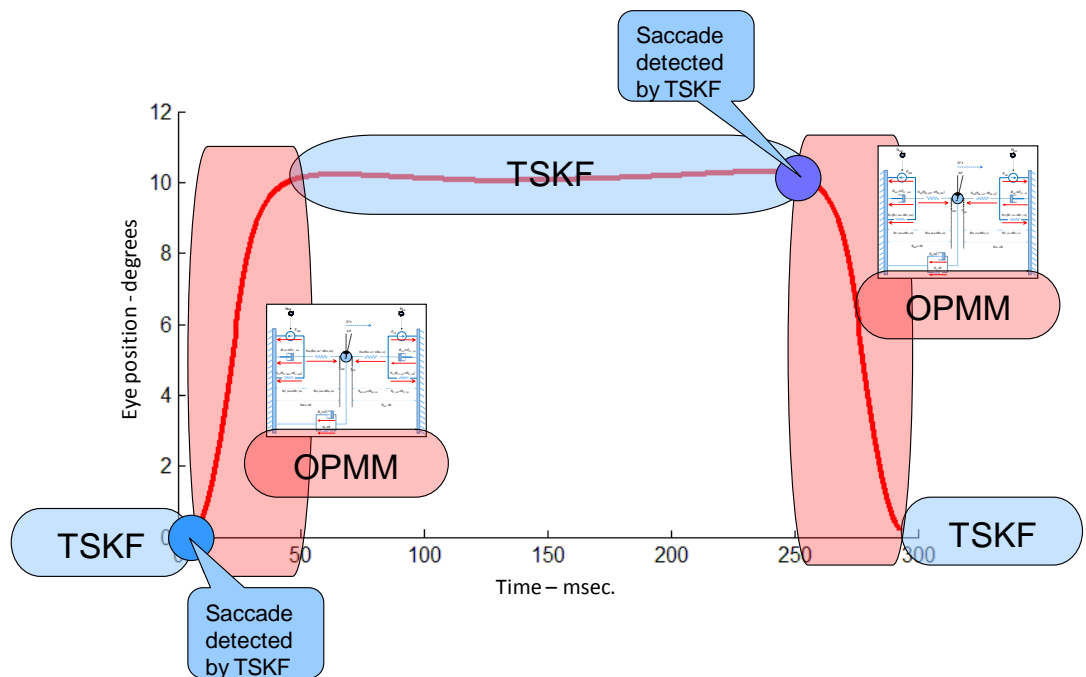


Fig. 16. Eye movement prediction by the OPMM model. The TSKF predicts eye movement trajectories during all eye movements except saccades. The OPMM predicts eye movement during saccades.

6.4.3 Oculomotor Plant Kalman Filter (OPKF)

The OPKF includes all of the components presented in Section 4.2. This means that the TSKF predicts eye movement trajectories during all eye movements except

saccades. Once a saccade is detected the Oculomotor Plant Mechanical Model transformed into the Kalman Filter form predicts the eye movement trajectory during the saccade.

The concept of eye movement prediction by the OPKF is diagrammatically represented in Fig. 17.

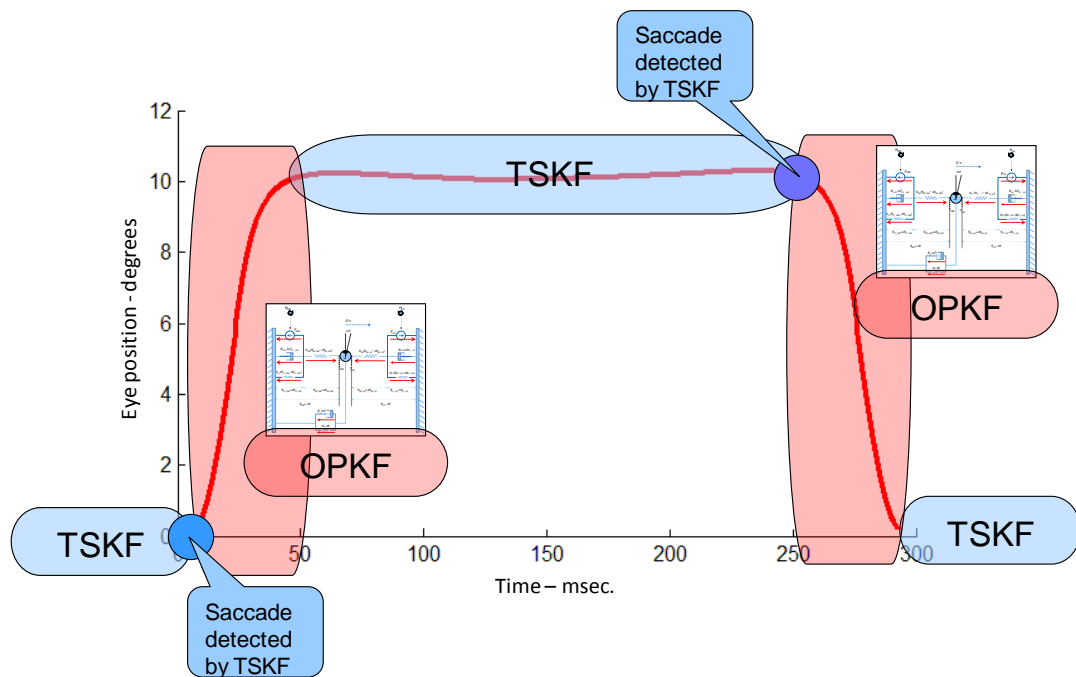


Fig. 17. Eye movement prediction by the OPKF model. The TSKF predicts eye movement trajectories during all eye movements except saccades. The OPMM in the Kalman Filter form predicts eye movements during saccades.

6.4.4 Oculomotor Plant Kalman Filter + (OPKF+)

The OPKF+ framework employs the Oculomotor Plant Mechanical Model presented in the Kalman Filter form for the additional 200 msec. after the end of every

saccade. This approach is based on the fact that the brain needs at least 200 msec. to calculate the parameters of the next saccade after the end of the previous saccade (Sparks, 2002). During these 200 msec. an eye remains in the state of fixation or pursuit. An eye movement trajectory predicted by the OPMM alone closely resembles a fixation trajectory. Thus, if the eye movement after the end of a saccade results in an eye fixation, then the prediction error between the measured eye position and the trajectory computed by the OPMM is going to be very small. If the eye movement after the end of the saccade is a smooth pursuit movement, then the prediction error is going to increase, but still the error will be less than if the prediction were done by the TSKF. This assumption was confirmed by our experiments.

The concept of eye movement prediction by the OPKF+ is diagrammatically represented in Fig. 18.

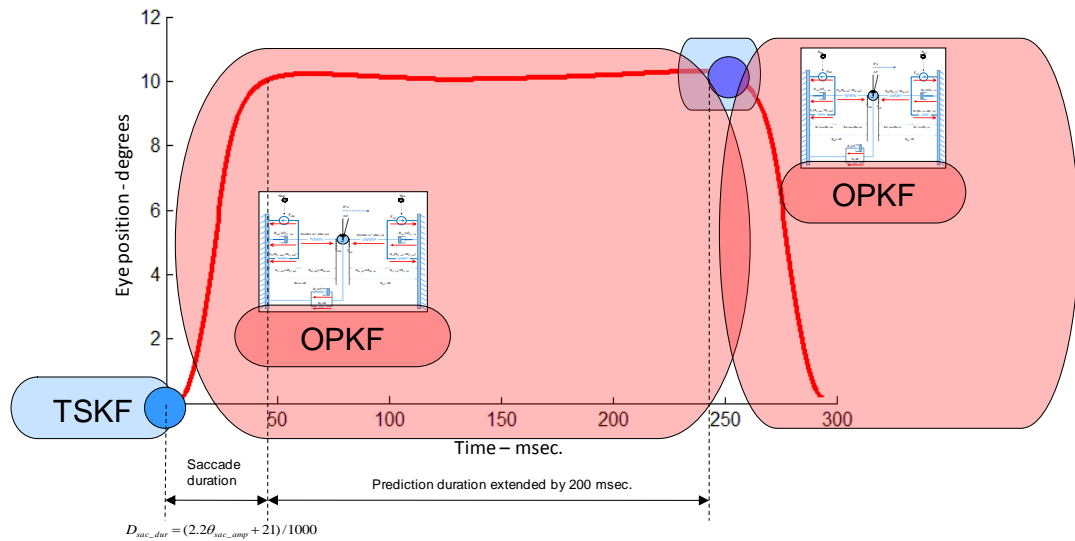


Fig. 18. Eye movement prediction by the OPKF+ model. The TSKF predicts eye movement trajectories during all eye movements except saccades. The OPMM in the Kalman Filter form predicts eye movements during saccades +200 msec. after the end of each saccade.

6.5 Evaluation

All prediction models were implemented in MATLAB. Eye movement recordings were analyzed off-line. From 63 recordings done for 21 subjects, 6 recordings were removed due to excessive noise. Standard deviation numbers reported in Fig. 19

through Figure 24 were calculated by the following formula $stdev = \sqrt{\frac{\sum(x-\bar{x})^2}{n-1}}$ where

n is the sample size and \bar{x} is the sample mean. The eye movement prediction was done only for the horizontal movement component of the right eye. In our experiments all eye movement prediction models predicted the eye movement trajectories 20 msec.

ahead.

6.6 Eye Movement Prediction Accuracy Metric

The root mean squared error (RMSE) between the predicted eye rotation $\hat{x}_1^-(k)$ calculated by Equation 36 and the measured eye position coordinate z_k computes the accuracy of an eye movement prediction. The RMSE values are computed for each eye movement type.

The RMSE was calculated using the following formula:

$$RMSE = \sum_{k=i}^j \frac{\sqrt{(\hat{x}_1^-(k) - z_k)^2}}{j - i} \quad (68)$$

where $\hat{x}_1^-(i)$ is the predicted eye tracker coordinate, calculated by Equation 36 and z_k is the eye position coordinate measured by the eye tracker. i and j create the size of the sampling window for each eye movement type. The ideal eye movement prediction model will have the RMSE of 0° .

The percentage improvement in prediction accuracy (reduction of the RMSE) between various eye movement prediction models is calculated by the following formula:

$$\Lambda = 100 \frac{RMSE_{Model_1} - RMSE_{Model_2}}{RMSE_{Model_1}} \quad (69)$$

where the $RMSE_{Model_1}$ was reported by the Model 1 and the $RMSE_{Model_2}$ was reported by the Model 2.

This Chapter presented a metric for measuring the accuracy of eye movement prediction and a video set used to test four eye movement prediction models.

CHAPTER 7

Results

This Chapter presents the results achieved by the four eye movement prediction models described in Section 6.4. The results are discussed in terms of various eye movement types and test videos. Possible methods of increasing the accuracy of eye movement prediction are presented. Also presented are eye movement predictions during eye tracking failures and real time capabilities of the eye movement prediction framework developed in this Dissertation.

7.1 Test Video Set Performance

Test video set eye movement data is presented in Fig. 19, Fig. 20, and Fig. 21.

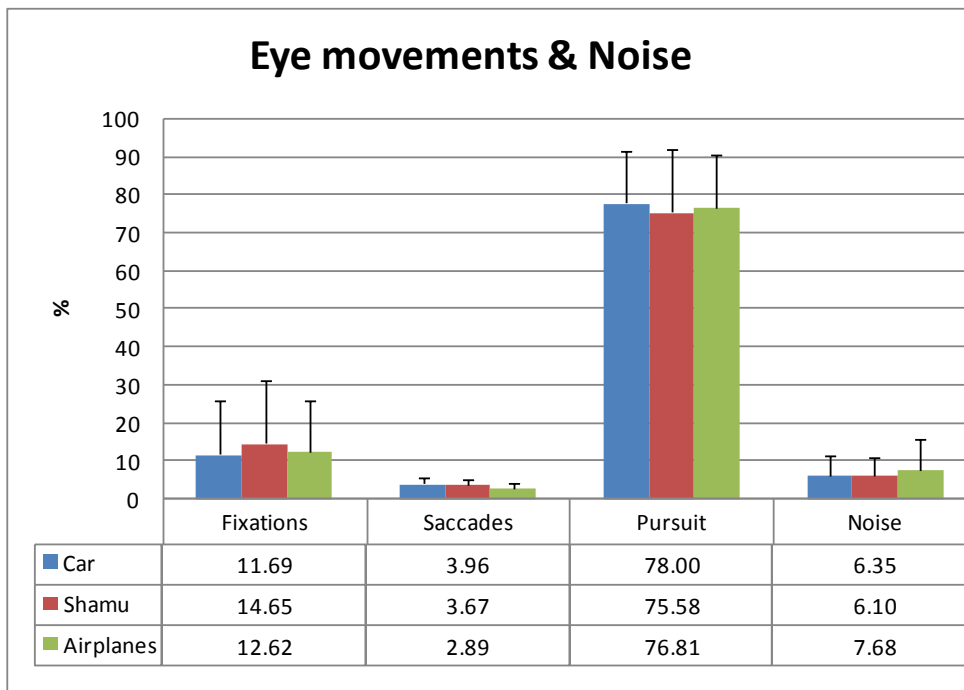


Fig. 19. Average percentage of the eye position samples that belong to a specific eye movement type and the average percentage of Not Reported eye position samples.

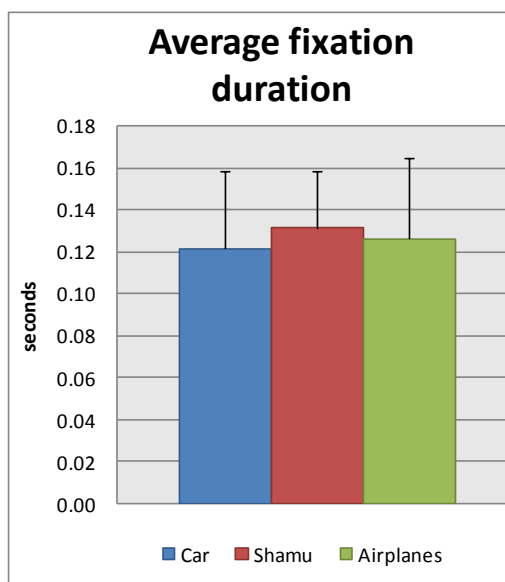


Fig. 20. Average fixation duration with standard deviation for each test video.

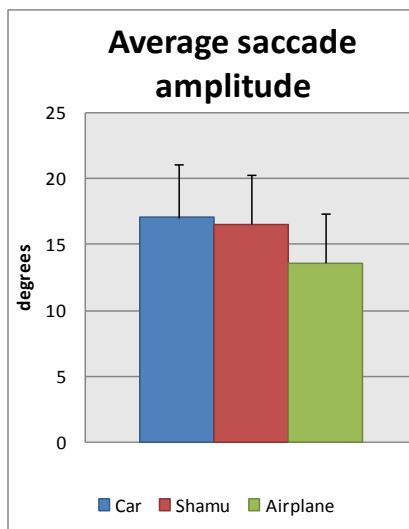


Fig. 21. Average saccade amplitude

with standard deviation for each test video.

Fixations:

The average amount of eye position samples belonging to fixations was 12-15%. “Shamu” had the highest number of eye fixations - 15%, “Car” and “Airplanes” had 12%. Standard deviation values varied significantly between video clips - from 13% to 15%. Two subjects’ recordings did not have any fixations detected by the IV-T model.

Average fixation duration results are presented in Fig. 20. These results indicate that the average eye fixation duration for all video clips was approximately 130 msec., deviating approximately 30-40 msec. from the mean.

Saccades:

The average percentage of saccadic eye movements was the smallest for “Airplanes” – approximately 3%, and approximately 4% for “Car” and “Shamu”

videos. The standard deviation among subjects for saccades was 1.56% for “Car”, 1.43% for “Shamu” and 1.32% for “Airplanes”.

The average saccade amplitude represented in Fig. 21 was around 17° for the “Car” and “Shamu” videos and 14° for the “Airplane” video. The standard deviation was approximately 4° from these values.

Smooth pursuits:

The average percentage of pursuit eye movements was the smallest for “Shamu” – 76%. “Airplanes” had 77% and “Car” – 78%. Standard deviation values for smooth pursuits mirrored eye fixation’s standard deviation values. This is explained by the fact that the groups of fixations and pursuits blend into each other, with samples from the fixation group going to the pursuit group and vice versa, based on the boundary of eye fixation detection criteria. The amount of saccadic eye movements remained almost constant throughout the experiments without affecting the fixation or the pursuit group.

Not Reported:

The Not Reported category presented in Fig. 19 is the percentage of eye position samples for which the eye tracker failed to report the eye position coordinates. The amount of such samples on average was between 5-8%.

As was mentioned previously each video clip had a different subjective “feel”, but surprisingly all three test videos on average triggered similar eye movement behavior. All three videos produced the large number of pursuit eye movements, a low number of

fixations and an extremely low number of saccadic eye movements. Even eye movement characteristics such as average saccade amplitude and eye fixation duration were similar for all three video clips. Still it can be pointed out that the “Car” video was more challenging to the HVS than were the other videos. This conclusion is supported by the higher saccade amplitudes, amplitude deviations and by the percentage of the saccadic eye movements recorded for the “Car” video. The least challenging video was “Airplanes” with the smallest number of saccades, smaller saccade amplitudes and smaller deviations.

The results show that the video challenge ranking calculated by the quantitative eye movement analysis differs from the ranking done by the subjective analysis.

7.2 Eye Movement Prediction Results

The RMSE results for each model are presented in Fig. 22, Fig. 23, and Figure 24. The prediction interval for each model was 20 msec.

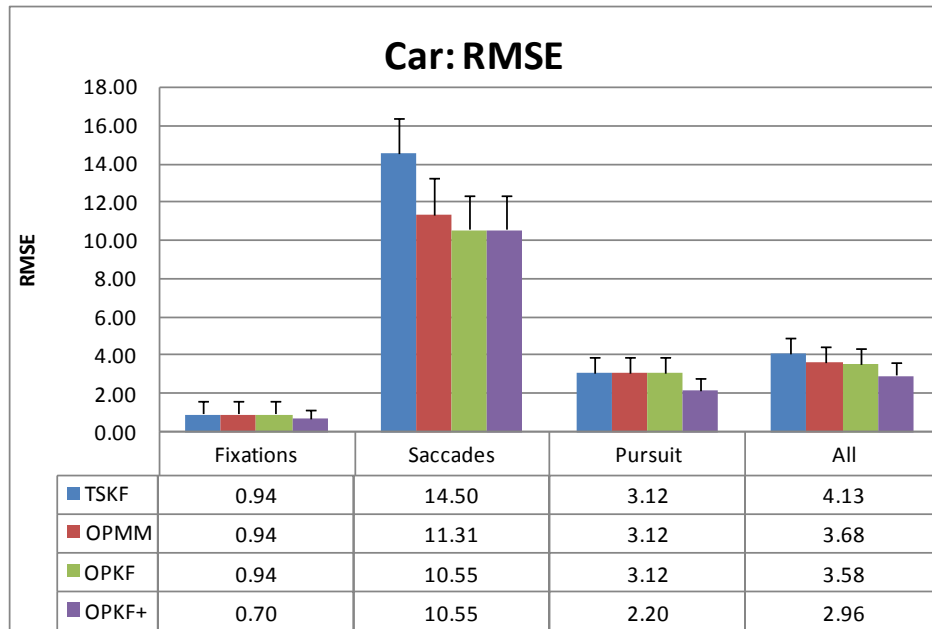


Fig. 22. Car video. The RMSE and RMSE standard deviations for four eye movement prediction models.

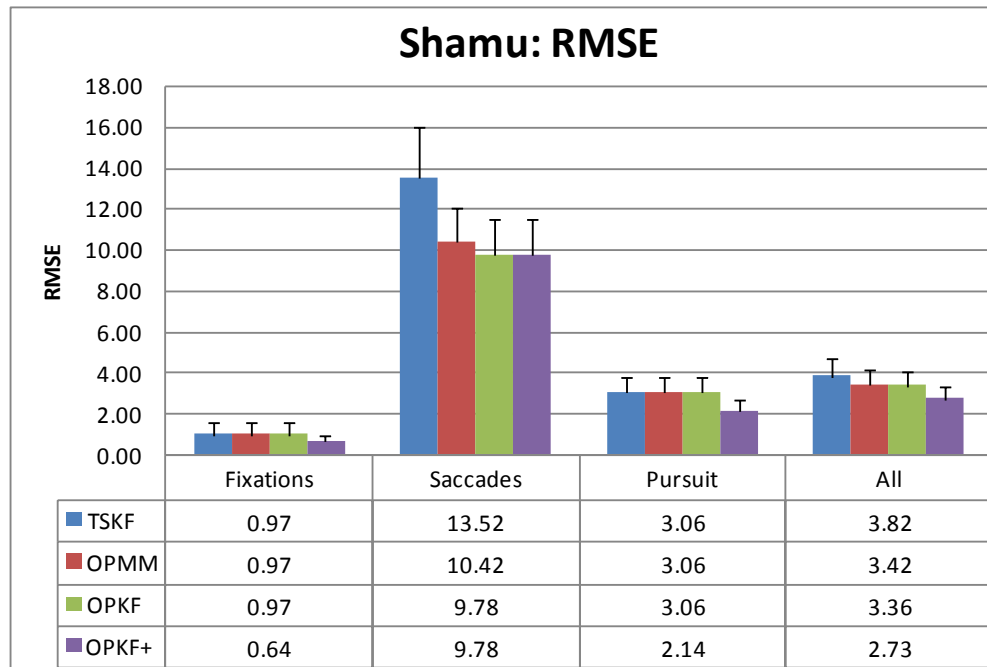


Fig. 23. Shamu video. The RMSE and RMSE standard deviations for four eye movement prediction models.

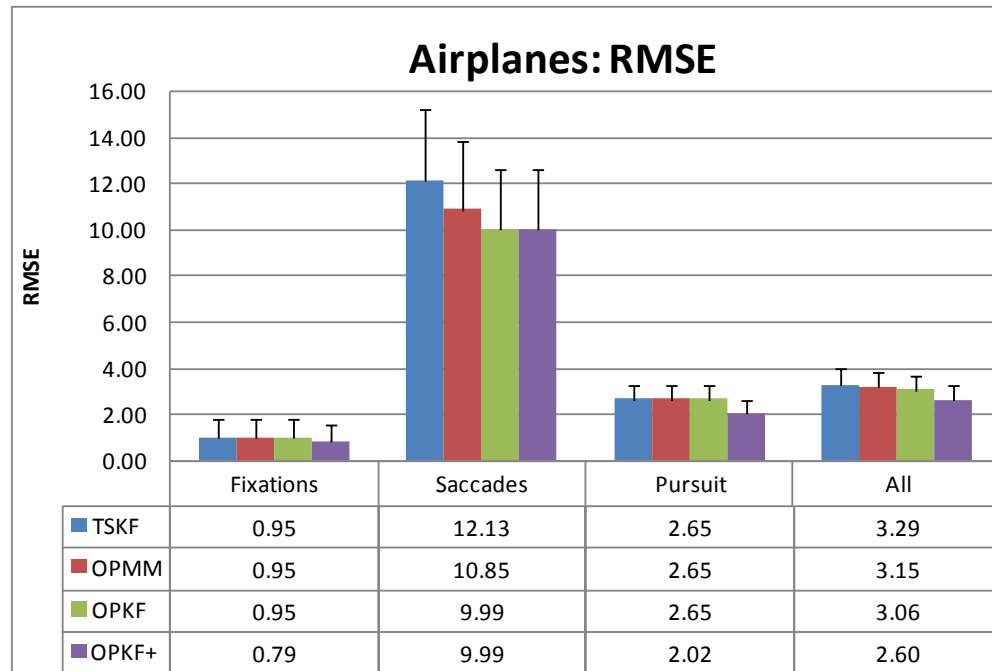


Figure 24. Airplanes video. The RMSE and RMSE standard deviations for four eye movement prediction models.

7.2.1 Fixations

I assume that the main source of the prediction error comes from the fact that the eye is not absolutely stationary during a fixation; there are various types of sub-movements during a fixation i.e. tremor, drift and involuntary saccades with amplitudes of up to 0.5° (Yarbus, 1967).

All prediction models maintained an RMSE below 1° for all video clips in the experiments.

Model specific results:

The TSKF, the OPMM, and the OPKF models produced an RMSE in the range of 0.94-0.97°. This result indicates that the Two State Kalman Filter modeling the Human Visual System through an eye position and velocity successfully predicts the eye movement trajectory during eye fixations. The OPKF+ model with more sophisticated bio modeling was capable of reducing the RMSE during fixations by 17-34%, bringing it down to 0.64-0.79°.

Video specific results:

Table 1 presents the RMSE values and the accuracy improvement values during fixations achieved by the OPKF+ model vs. the TSKF model.

Fixations	TSKF	OPKF+	Accuracy improvement
"Car"	0.94	0.70	26%
"Shamu"	0.97	0.64	34%
"Airplanes"	0.95	0.79	17%

Table 1. Fixations. The RMSE values and the prediction accuracy improvement between the TSKF and the OPKF+ models.

The improvement in the prediction accuracy achieved by the OPKF+ during fixations is correlated to the percentage of the saccades in the eye movement trace. A high number of saccades results in more frequent use of the bio-aware Oculomotor Plant Mechanical Model, which ensures the improvement of the accuracy of prediction. This conclusion is supported by the fact that in the “Car” and the “Shamu” videos,

where the number of saccades is the highest (~4%), the improvement in the prediction accuracy is 26-34% as compared to a 17% improvement in the predicted accuracy in the “Airplanes” video where the number of saccades is the lowest (~3%).

7.2.2 Saccades

Saccades are the most challenging eye movement to predict due to their velocity, direction, and amplitude.

All prediction models maintained an RMSE in the range of 9.78-14.5°.

Model specific results:

The TSKF produced an RMSE of 12.77-14.5°, with a standard deviation of 2.33-3.11°. This result indicates that the Two State Kalman Filter modeling the Human Visual System through eye position and velocity is a poor predictor during saccades.

The OPMM reduced the RMSE by 11-22%, bringing the range of error down to 10.85-11.31°. This result indicates that the Oculomotor Plant Mechanical Model with a prediction mechanism but without noise modeling and measurement from the eye tracker, significantly improves the prediction accuracy achieved by the TSKF during saccades.

The OPKF reduced the RMSE by 7-28%, down to 9.78-10.55° on top of the performance already achieved by the OPMM. This significant margin of improvement is achieved by the OPKF by presenting the OPMM in the Kalman Filter form that

models system's and measurement noise and uses updates from the eye tracker.

The OPKF+ has the same performance as the OPKF during saccades.

Video specific results:

Table 2 presents the RMSE values and the accuracy improvement values during saccades achieved by the OPKF+ model vs. the TSKF model.

Saccades	TSKF	OPKF+	Accuracy improvement
"Car"	14.50	10.55	27%
"Shamu"	13.52	9.78	28%
"Airplanes"	12.13	9.99	18%

Table 2. Saccades. The RMSE values and the prediction accuracy improvement between the TSKF and the OPKF+ models.

Due to the highest error it is possible to conclude that the "Car" was the most challenging video for all prediction models in terms of saccade trajectory prediction.

In the case of the "Airplanes" video the improvement in the accuracy of the prediction was the smallest. It was assumed that this occurred because the saccades exhibited by subjects had small amplitudes. The average saccade amplitude for "Airplanes" was approximately 14° , while "Car" and "Shamu" had average saccade amplitudes of approximately 17° . The accuracy improvement achieved by the mechanical modeling of the eye is most effective for saccades of large amplitudes.

A valid question to ask is what are the factors limiting further improvements in the prediction accuracy achieved by the OPKF framework? At least one of those factors is tied to how soon a saccade can be detected by the TSKF component of the OPKF

framework. Given an eye position sampling frequency of 50Hz the experiments indicate that the chi square test detects a saccade usually with the first measured eye position sample that is available after the beginning of the saccade. This allows the OPMM component inside the OPKF framework to make the first eye movement trajectory prediction only for the next eye position coordinate following the saccade detection. This means that 20-40 msec. at the beginning of every saccade is predicted by the position/velocity model (TSKF) instead of by the bio mechanical model (OPMM). As seen from the results the TSKF is not very accurate in predicting saccadic eye movements. My conclusion is the higher the eye position sampling frequency, the sooner saccade parameters can be estimated by the OPKF, thus improving the prediction accuracy.

7.2.3 Pursuits

Pursuits have less velocity than saccades and thus they are easier to predict.

All prediction models maintained an RMSE in the range of 2.65-3.12°.

Model specific results:

The TSKF, the OPMM, and the OPKF models produced RMSE in the range of 2.65-3.12°. This result indicates that the Two State Kalman Filter is less successful in predicting an eye movement trajectory during the smooth pursuits than during the fixations, but more successful than during the saccades. The OPKF+ model with more

sophisticated bio modeling was capable of reducing the RMSE during fixations by 21-29%, bringing it down to 2.02-2.20°.

Video specific results:

Table 3 presents the RMSE values and the accuracy improvement values during pursuits achieved by the OPKF+ model vs. the TSKF model.

Pursuits	TSKF	OPKF+	Accuracy improvement
"Car"	3.12	2.20	29%
"Shamu"	3.06	2.14	30%
"Airplanes"	2.65	2.02	24%

Table 3. Pursuits. The RMSE values and the prediction accuracy improvement between the TSKF and the OPKF+ models.

The improvement in the prediction accuracy achieved by the OPKF+ during pursuits is correlated to the percentage of saccades in the eye movement trace. A high number of saccades results in more frequent use of the bio-aware Oculomotor Plant Mechanical Model, which ensures the improvement of the accuracy of prediction. This assumption is supported by the fact that in the “Car” and the “Shamu” videos where the amount of saccades is the highest (~4%), the improvement in the prediction accuracy is 29-30% as compared to a 21% improvement in the predicted accuracy in the “Airplanes” video where the number of saccades is the lowest (~3%).

7.2.4 All Eye Movements Combined

The “All” category calculated the overall performance of each prediction model.

This goal was achieved by calculating the RMSE for all eye position samples except Not Reported.

Model specific results:

The TSKF produced the largest RMSE of 3.29-4.13° with the largest standard deviation of 0.69-1°.

The OPMM model reduced the RMSE by 4-11%, down to 3.15-3.68° and the standard deviation by 2-19%, down to 0.66-0.8°.

The OPKF model reduced the RMSE on top of the OPMM by 2-3% with values of 3.06-3.58°. The standard deviation was reduced by 3-4% for “Car” and “Airplanes”. The standard deviation for the “Shamu” video increased by 0.18%.

The OPKF+ model reduced the RMSE on top of the OPKF by 15-19% with values of 2.60°-2.96°. Standard deviation was decreased by 11-15% for “Car” and “Shamu”. The standard deviation for the “Airplanes” video increased by 1.18%.

These results signify that the OPKF+ model reduced the overall RMSE by 21%-30% and the RMSE standard deviation by 6%-30% compared to the base TSKF model.

According to the results, the first significant accuracy improvement was achieved by adding the Oculomotor Plant Mechanical Model to the Two State Kalman Filter (an improvement of 4-11%). The second significant accuracy improvement was achieved by enhancing the Oculomotor Plant Kalman Filter model by extending the use of the OPMM by an additional 200 msec. after each saccade (an improvement of 15-19%).

Overall the highest improvement of prediction accuracy occurs during saccades. In

the presented test video set the number of saccades was 3-4%. My conclusion is that if the amount of saccades in the eye movement trace is increased, the overall margin of improvement between the TSKF and the OPKF+ models will increase as well.

Video specific results:

Table 4 presents the RMSE values and the accuracy improvement values during all eye movements achieved by the OPKF+ model vs. the TSKF model.

All	TSKF	OPKF+	Accuracy improvement
"Car"	4.13	2.96	28%
"Shamu"	3.82	2.73	29%
"Airplanes"	3.29	2.60	21%

Table 4. All eye movements. The RMSE values and the prediction accuracy improvement between the TSKF and the OPKF+ models.

The “Car” video had the highest prediction error from three videos, that it why it is possible to conclude that it was the most challenging video.

7.2.5 Statistical Significance

The statistical significance of the accuracy improvement between four eye movement prediction models was tested for “All” category with a t-test. It was assumed that test populations were normally distributed having the variances that are unknown and assumed to be unequal.

The null hypothesis was formulated as follows: $H_0: \mu_{model_1} - \mu_{model_2} \leq 0$ where μ_{model_1} is the sample mean of RMSE values reported by eye movement prediction

model 1 and μ_{model_2} is the sample mean reported for the model 2. The alternative hypothesis is $H_a: \mu_{model_1} - \mu_{model_2} > 0$.

With these assumptions the statistical significance results of the accuracy improvement between models is presented in Table 5.

Models	Level of significance	t-test results
OPMM vs. TSKF	0.01	all videos passed
OPKF vs. OPMM	0.1	"Shamu" failed; "Car" and "Airplanes" passed
OPKF+ vs. OPKF	0.01	all videos passed
OPKF+ vs. TSKF	0.01	all videos passed

Table 5. t-test results.

7.3 Eye Movement Prediction during Eye Tracking Failures

An eye position sample was classified as Not Reported when the eye tracker failed to report the proper eye position coordinates. The failure to identify the correct eye position coordinates usually occurred due to the subject's blinking, jerky head movements, changes in the content's lighting, excessive wetting of the eye, and squinting. The amount of Not Reported eye position samples varied between 3-33% per experiment. In the cases in which the tracking failed for a brief period of time, the OPKF framework was still capable of predicting eye movement trajectories by using the measurement noise covariance matrix defined by Equation 63.

Fig. 25 presents an example of eye movement prediction by the OPKF during eye tracking failures.

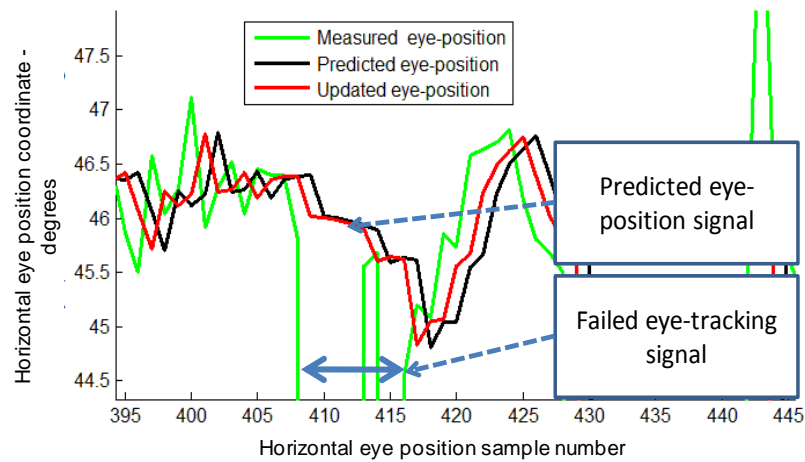


Fig. 25. Eye movement prediction by the Two State Kalman Filter during two eye tracking failures.

7.4 Real-time Performance

The OPKF is a linear six order system. The OPKF real-time performance comes from the fact that most computationally expensive calculations performed by the OPKF are matrix operations within the Kalman Filter framework. Modern computers can perform all necessary types of operations for 6x6 matrixes in real-time.

7.5 Future Improvement of Prediction Accuracy

Further research in improving eye movement prediction accuracy for the type of the multimedia tested in this Dissertation, should come from the development of the neuronal control signal and the active state tension models for smooth pursuit eye movements. In the experiments presented in this Dissertation the amount of smooth

pursuit movement was 76-78%, thus any improvement in the accuracy of prediction during smooth pursuit will result in a significant overall increase in prediction accuracy.

This Chapter has presented the performance results achieved by the four eye movement prediction models. The performance data was evaluated in terms of basic eye movement types and test videos. The chapter has discussed such issues as eye movement trajectory predictions during eye tracking failures, real-time performance of the OPKF framework and ways of improving eye movement prediction accuracy in future research.

CHAPTER 8

Conclusion

Eye tracking technology can successfully enhance already existing interaction methods. There are several issues that need to be resolved before this can happen. One of these issues is related to the fact that interactive systems are frequently deployed in network environments that introduce various types of delay. If the delay is not compensated for, a system's responsiveness will decrease and interaction errors will occur. The second issue of eye tracking is time intervals during which an eye tracker fails to report eye position coordinates. Usually such failures are short and they occur due to a subject blinking, exhibiting jerky head movements, etc. Such failures lead to interaction errors.

This Dissertation has created a mechanical model of the human eye that can be used for eye movement prediction. Presented in the Kalman Filter form, this model enables continuous prediction of the eye movement signal. This approach addresses the issue of the delay compensation and eye tracking failures. This Dissertation has presented four distinct eye movement prediction models: TSKF – the position and velocity model, without the knowledge of eye anatomy; OPMM – the model that represents eye anatomical properties with their mechanical equivalents and uses an eye mechanical model for prediction; OPKF – the model that transforms the OPMM into

the Kalman Filter form, accounting for measurement noise and system noise properties; OPKF+ - the model that uses the OPKF as a base and incorporates the computational limitations of the brain to improve the accuracy of the eye movement prediction. The best performing model, the OPKF+, reported an the average prediction accuracy of approximately 2.6° - 2.96° for the 20 ms. delay range when using the tested multimedia files and 21 subjects. This was a 21-28% prediction accuracy improvement over the base TSKF model.

BIBLIOGRAPHY

Bahill, A. T. (1980). Development, validation and sensitivity analyses of human eye movement models. *CRC Critical Reviews in Bioengineering* , 4, 311-355.

Bahill, A. T., Latimer, J. R., & Troost, B. T. (1980). Linear homeomorphic model for human movement. *IEEE Trans. Biomed. Eng.* , 27, 631-639.

Brown, R., & Hwang, P. (1997). *Introduction to Random Signals and Applied Kalman Filtering* (3rd Edition ed.). New York: John Wiley and Sons.

Carmy, R., & Itti, L. (2006). Casual Saliency Effects During Natural Vision. *Symposium on Eye Tracking Research & Applications 2006 (ETRA 06)*, (pp. 11-18). San Diego.

Carpenter, R. H. (1977). *Movements of the Eyes*. London: Pion.

Collins, C. C. (1975). The human oculomotor control system. (F. Lennerstrand, & P. Bach-Rita, Eds.) *Basic Mechanisms of Ocular Motility and Their Applications* , 145-180.

Duchowski, A. T. (2003). *Eye Tracking Methodology: Theory and Practice*. London: Springer-Verlag.

Grinding, T. (2006, August). Eye Movement Analysis and Prediction with the Kalman Filter. *Masters Thesis* . Clemson, SC, USA: Computer Science Department, Clemson University.

Hill, A. V. (1938). The heat of shortening and dynamic constants of muscle. *Proc. Roy. Soc. B.* , 126, 136-195.

Hinkley, D. V. (1971). Inference about the change point from cumulative sum-tests. *Biometrika* , 59, 509-523.

Hsu, F. K., Bahill, A. T., & Stark, L. (1976). Parametric sensitivity analysis of a homeomorphic model for saccadic and vergence eye movements. *Computer Programs in Biomedicine* , 6, 108-116.

Jacob, K. R. (1995). *Eye tracking in advanced interface design*. New York: Oxford University Press, Inc.

Khan, J., & Komogortsev, O. V. (2006). A Hybrid Scheme for Perceptual Object Window Design with Joint Scene Analysis and Eye-Gaze Tracking for Media Encoding based on Perceptual Attention. *Journal of Electronic Imaging* , 15(2), 023018-01 - 023018-02.

Kohler, M. (1997). *Using the Kalman Filter to track Human Interactive Motion -- Modeling and Initialization of the Kalman Filter for Translational Motion*. Research Report No. 629, Universitt Dortmund, Fachbereich Informatik, 44221 Dortmund, Germany.

Komogortsev, O. V. (2007, May 22). *World of Warcraft Percept Interface*. Retrieved May 22, 2007, from World of Warcraft Percept Interface: <http://www.cs.kent.edu/~okomogor/wowpercept/wowpercept.htm>

Komogortsev, O. V., & Khan, J. (2007). Kalman Filtering in the Design of Eye-Gaze-Guided Computer Interfaces. *12th International Conference on Human-Computer Interaction (HCI 2007)*, (pp. 1-10). Beijing, China.

Komogortsev, O. V., & Khan, J. (2006). Perceptual Attention Focus Prediction for Multiple Viewers in Case of Multimedia Perceptual Compression with Feedback Delay. *Symposium on Eye Tracking Research & Applications 2006 (ETRA 06)*, (pp. 101-108). San Diego.

Komogortsev, O. V., & Khan, J. (2007). Perceptual Multimedia Compression based on the Predictive Kalman Filter Eye Movement Modeling. *Multimedia Computing and Networking Conference (MMCN'07)*, (pp. 1-12). San Jose.

Komogortsev, O. V., & Khan, J. (2004). Predictive Perceptual Compression for Real Time Video Communication. *12th ACM International conference on Multimedia (ACM MM 04)*, (pp. 220-227). New York.

Levin, A. W. (1927). The viscous elastic properties of a muscle. *Proc. R. Soc. London Ser. B.* , 108-115 .

Marin, C., & Schovanec, L. (1999). The control and mechanics of human movement systems. *Progress in Systems and Control Theory* , 25, 173-202.

Murphy, H., & T., D. A. (2001). Gaze-Contigent Level Of Detail Rendering. *Eurographics*.

Murtagh, F., Farid, M., & Starck, J. L. (2002). Computer display control and interaction using eye-gaze. *Journal of the Society for Information Display* , 10(3), 289-293.

Partala, T., Jokiniemi, M., & Surakka, V. (2001). Combined voluntary gaze direction and facial muscle activity as a new pointing technique. *INTERACT'2001*, (pp. 100-107).

Peters, R., & Itti, L. (2006). Computational mechanism for gaze direction in interactive visual environments. *Symposium on Eye tracking Research & Applications 2006 (ETRA 06)*, (pp. 27-32). San Diego.

Robinson, D. A. (1973). Models of the saccadic eye movement control system. *Kybernetik* , 14(2), 71-83.

Robinson, D. A., Omeara, D. M., Scott, A. B., & Collins, C. C. (1969). Mechanical components of human eye movements. *Journal of Applied Physiology* , 548-553.

Salvucci, D. D., & Anderson, J. R. (2000). Intelligent gaze-added interfaces. *SIGCHI Conference on Human Factors in Computing Systems (CHI '00)* (pp. 273-280). New York: ACM Press.

Salvucci, D. D., & Goldberg, J. H. (2000). Identifying fixations and saccades in eye tracking protocols. *Eye Tracking Research and Applications Symposium* (pp. 71-78). New York: ACM Press.

Sauter, D., J., M. B., Di Renzo, N., & Vomscheid, C. (1991). Analysis of eye tracking movements using innovations generated by a Kalman filter. *Med. Biol. Eng. Comput.* , 63–69.

Shebilske, W. L., & Fisher, D. F. (1983). Understanding Extended Discourse Through the Eyes: How and Why. (D. F. Fisher, R. Groner, C. Menz, & R. A. Monty, Eds.) *Eye Movements and Psychological Functions: International Views* , 303-314.

Sparks, D. L. (2002). The brainstem control of saccadic eye movements. *Nat. Rev. Neurosci.* , 3(12), 952-964.

Stelmach L. B.; Tam W. J. (1994). Processing image sequences based on eye movements. *Human Vision, Visual Processing, and Digital Display V. 2179*, pp. 90-98. SPIE.

Tsumura, N., Endo, C., Haneishi, H., & Miyake, Y. (1996). Image compression and decompression based on gazing area. *Human Vision and Electronic Imaging*. SPIE.

Wang, Z., & Bovik, A. C. (2001). Embedded foveation image coding. *IEEE Transactions on Image Processing* , 10, 1397-1410.

Ware, C., & Mikaelian, H. T. (1987). An Evaluation of an Eye Tracker as a Device for Computer Input. *ACM CHI+GI'87 Human Factors in Computing Systems Conference*, (pp. 183-188).

Westheimer, G. (1954). Mechanism of saccadic eye movements. *A.M.A. Archives of Ophthalmology* , 52, 710-724.

Wilkie, D. R. (1976). Muscle. *Studies in Biology* , 11.

Yanoff, M., & Durker, J. (1999). *Ophthalmology*. Mosby International Ltd.

Yarbus, L. (1967). *Eye Movements and Vision*. Moscow: Institute for Problems of Information Transmission Academy of Sciences of the USSR.

GLOSSARY

I-VT	Velocity-Threshold Identification
MMM	Muscle Mechanical Model
OPKF	Oculomotor Plant Kalman Filter
OPKF+	Oculomotor Plant Kalman Filter Enhanced
OPMM	Oculomotor Plant Mechanical Model
TSKF	Two State Kalman Filter

APPENDIX A

A.1 Agonist Muscle Mechanical Model of Lateral Rectus

Equations 1 and 2 can be combined into the equation:

$$-K_{SE}(\theta_{SE_LR} + \Delta\theta_{SE_LR}) + F_{LR} + K_{LT}(\theta_{LT_LR} - \Delta\theta_{LT_LR}) - B_{AG}\Delta\dot{\theta}_{LT_LR} = 0 \quad (70)$$

Taking into consideration that $\theta_{LR} = \theta_{LT_LR} + \theta_{SE_LR}$ and $\Delta\theta = \Delta\theta_{LT_LR} - \Delta\theta_{SE_LR}$ the following equation can be calculated:

$$\theta_{LR} - \Delta\theta = \theta_{LT_LR} + \theta_{SE_LR} - \Delta\theta_{LT_LR} + \Delta\theta_{SE_LR} \quad (71)$$

rearranging the previous equation we get:

$$\theta_{SE_LR} + \Delta\theta_{SE_LR} = \theta_{LR} - \Delta\theta - \theta_{LT_LR} + \Delta\theta_{LT_LR} \quad (72)$$

Combining Equations 70 and 72

$$-K_{SE}(\theta_{LR} - \Delta\theta - \theta_{LT_LR} + \Delta\theta_{LT_LR}) + F_{LR} + K_{LT}(\theta_{LT_LR} - \Delta\theta_{LT_LR}) - B_{AG}\Delta\dot{\theta}_{LT_LR} = 0 \quad (73)$$

$$-K_{SE}(\Delta\theta_{LT_LR} - \Delta\theta) + (F_{LR} - K_{SE}(\theta_{LR} - \theta_{LT_LR}) + K_{LT}\theta_{LT_LR}) - K_{LT}\Delta\theta_{LT_LR} \quad (74)$$

$$- B_{AG}\Delta\dot{\theta}_{LT_LR} = 0$$

assigning $\hat{F}_{LR} = F_{LR} - K_{SE}(\theta_{LR} - \theta_{LT_LR}) + K_{LT}\theta_{LT_LR}$ Equation 74 can be re-written as:

$$K_{SE}(\Delta\theta_{LT_LR} - \Delta\theta) = \hat{F}_{LR} - K_{LT}\Delta\theta_{LT_LR} - B_{AG}\Delta\dot{\theta}_{LT_LR} \quad (75)$$

New equations for T_{LR} can be written as:

$$T_{LR} = K_{SE}(\Delta\theta_{LT_LR} - \Delta\theta) \quad (76)$$

$$T_{LR} = \hat{F}_{LR} - K_{LT}\Delta\theta_{LT_LR} - B_{AG}\Delta\dot{\theta}_{LT_LR} \quad (77)$$

Using Equation 76 $\Delta\theta_{LR}$ can be calculated as $\Delta\theta_{LT_LR} = \frac{T_{LR}}{K_{SE}} + \Delta\theta$. This result can be substituted into Equation 77 to calculate:

$$T_{LR} = \hat{F}_{LR} - K_{LT}\left(\frac{T_{LR}}{K_{SE}} + \Delta\theta\right) - B_{AG}\Delta\dot{\theta}_{LT_LR} \quad (78)$$

Equation 78 can be transformed into:

$$T_{LR} = \frac{\hat{F}_{LR}K_{SE}}{K_{SE} + K_{LT}} - \frac{\Delta\theta K_{SE}}{K_{SE} + K_{LT}} - \frac{B_{AG}K_{SE}}{K_{SE} + K_{LT}}\Delta\dot{\theta}_{LT_LR} \quad (79)$$

By assigning $\hat{B}_{AG} = \frac{B_{AG}K_{SE}}{K_{SE} + K_{LT}}$ Equation 79 can be written in the form of:

$$T_{LR} = \frac{\hat{F}_{LR}K_{SE}}{K_{SE} + K_{LT}} - \frac{\Delta\theta K_{SE}}{K_{SE} + K_{LT}} - \hat{B}_{AG}\Delta\dot{\theta}_{LT_LR} \quad (80)$$

Equations 76 and 80 are the same as Equations 3 and 4.

A.2 Antagonist Muscle Mechanical Model of Medial Rectus

Equations 5 and 6 can be combined into the equation:

$$K_{SE}(\theta_{SE_MR} + \Delta\theta_{SE_MR}) - F_{MR} - K_{LT}(\theta_{LT_MR} + \Delta\theta_{LT_MR}) - B_{ANT}\Delta\dot{\theta}_{LT_MR} = 0 \quad (81)$$

Taking into consideration that $\theta_{MR} = \theta_{LT_MR} + \theta_{SE_MR}$ and $\Delta\theta = \Delta\theta_{LT_MR} - \Delta\theta_{SE_MR}$ the following equation can be calculated:

$$\theta_{MR} + \Delta\theta = \theta_{LT_MR} + \theta_{SE_MR} + \Delta\theta_{LT_MR} + \Delta\theta_{SE_MR} \quad (82)$$

Rearranging the previous equation we get:

$$\theta_{SE_MR} + \Delta\theta_{SE_MR} = \theta_{MR} - \theta_{LT_MR} + \Delta\theta - \Delta\theta_{LT_MR} \quad (83)$$

Combining Equations 81 and 83.

$$K_{SE}(\theta_{MR} - \theta_{LT_MR} + \Delta\theta - \Delta\theta_{LT_MR}) - F_{MR} - K_{LT}(\theta_{LT_MR} + \Delta\theta_{LT_MR}) - B_{ANT}\Delta\dot{\theta}_{LT_MR} = 0 \quad (84)$$

$$K_{SE}(\Delta\theta - \Delta\theta_{LT_MR}) - F_{MR} - K_{SE}\theta_{LT_MR} + K_{SE}\theta_{MR} - K_{LT}\theta_{LT_MR} - K_{LT}\Delta\theta_{LT_MR} - B_{ANT}\Delta\dot{\theta}_{LT_MR} = 0 \quad (85)$$

assigning $\hat{F}_{MR} = F_{MR} + K_{SE}\theta_{LT_MR} - K_{SE}\theta_{MR} + K_{LT}\theta_{LT_MR}$ Equation 85 can be re-written as:

$$K_{SE}(\Delta\theta - \Delta\theta_{LT_MR}) = \hat{F}_{MR} + K_{LT}\Delta\theta_{LT_MR} + B_{ANT}\Delta\dot{\theta}_{LT_MR} \quad (86)$$

$$-K_{SE}(\Delta\theta - \Delta\theta_{LT_MR}) = -\hat{F}_{MR} - K_{LT}\Delta\theta_{LT_MR} - B_{ANT}\Delta\dot{\theta}_{LT_MR} \quad (87)$$

New equations for T_{LR} can be written as:

$$T_{MR} = -K_{SE}(\Delta\theta - \Delta\theta_{LT_MR}) \quad (88)$$

$$T_{MR} = -\hat{F}_{MR} - K_{LT}\Delta\theta_{LT_MR} - B_{ANT}\Delta\dot{\theta}_{LT_MR} \quad (89)$$

Using Equation 88 $\Delta\theta_{LT_MR}$ can be calculated as $\Delta\theta_{LT_MR} = \Delta\theta + \frac{T_{MR}}{K_{SE}}$. This result can be substituted into Equation 89 to calculate:

$$T_{MR} = -\hat{F}_{MR} - K_{LT}\left(\Delta\theta + \frac{T_{MR}}{K_{SE}}\right) - B_{ANT}\Delta\dot{\theta}_{LT_MR} \quad (90)$$

Equation 90 can be transformed into:

$$T_{MR} = -\frac{\hat{F}_{MR}K_{SE}}{K_{SE} + K_{LT}} - \frac{\Delta\theta K_{SE}}{K_{SE} + K_{LT}} - \frac{B_{AG}K_{SE}}{K_{SE} + K_{LT}}\Delta\dot{\theta}_{LT_MR} \quad (91)$$

By assigning $\hat{B}_{ANT} = \frac{B_{ANT}K_{SE}}{K_{SE} + K_{LT}}$ Equation 91 can be rewritten as:

$$T_{MR} = -\frac{\hat{F}K_{SE}}{K_{SE} + K_{LT}} - \frac{\Delta\theta K_{SE}}{K_{SE} + K_{LT}} - \hat{B}_{ANT}\Delta\dot{\theta}_{LT_MR} \quad (92)$$

Equations 88 and 92 are the same as Equations 7 and 8.

A.3 Oculomotor Plant Mechanical Model – Negative Amplitude Saccades

Saccades of negative amplitude are performed by the medial rectus as the agonist and the lateral rectus as the antagonist. Next, a Mechanical Muscle Model will be presented for the medial rectus acting as the agonist and the lateral rectus acting as the antagonist.

Agonist Muscle Mechanical Model of Medial Rectus

The agonist muscle contracts, rotates the eye globe and stretches the antagonist muscle. Assuming that the medial rectus plays the role of the agonist we can present the MMM of the agonist muscle pulling the eye-globe in the negative direction in Fig. 26. The original length of the displacement in the series elasticity spring and length tension spring added together is θ_{MR} . The right eye moves to the left by $\Delta\theta$. $\Delta\theta$ is a negative number measured in degrees. The original displacement θ_{MR} is reduced making the resulting displacement $\theta_{LR} + \Delta\theta$. $\Delta\theta = -\Delta\theta_{SE_LR} + \Delta\theta_{LT_LR}$. Both $\Delta\theta_{SE_LR}$ and $\Delta\theta_{LT_LR}$ are negative numbers. Muscle contraction expands the series elastic component making resulting displacement $\theta_{SE_LR} - \Delta\theta_{SE_LR}$. Muscle contraction shortens the length tension component making the resulting displacement $\theta_{LT_LR} + \Delta\theta_{LT_LR}$. The damping

component modeling the force velocity relationship $-B_{AG}\Delta\dot{\theta}_{LT_LR}$ resists the muscle contraction. The negative sign in front of the damping component makes the value of force positive as represented by $B_{AG}\Delta\dot{\theta}_{LT_LR}$.

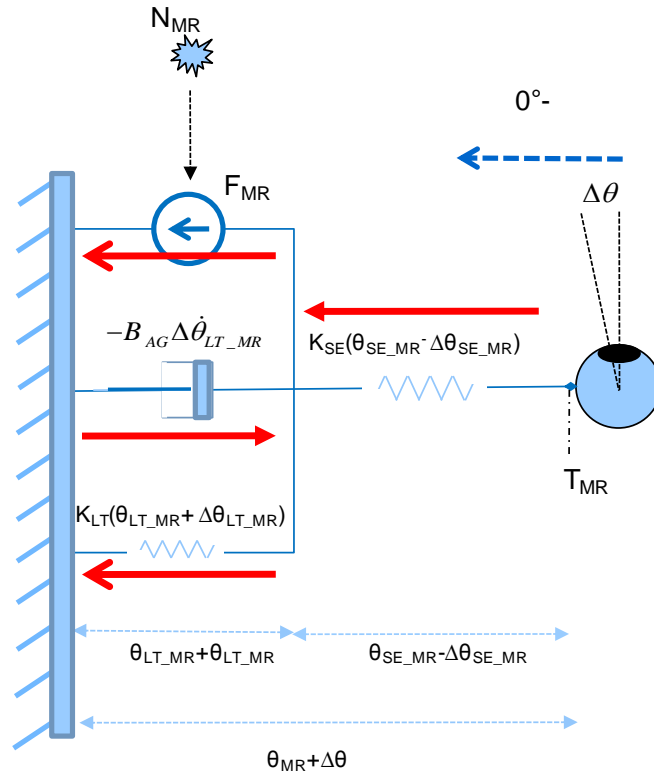


Fig. 26. Agonist Muscle Mechanical Model of Medial Rectus. Arrows represent the direction of the forces.

Using Fig. 26, we can write the equation of force with which the part of the diagram responsible for contraction (active state tension, damping component, length tension component) pulls the series elasticity component.

$$T_{MR} = -F_{MR} - K_{LT}(\theta_{LT_MR} + \Delta\theta_{LT_MR}) + (-B_{AG}\Delta\dot{\theta}_{LT_MR}) \quad (93)$$

Resisting the contraction series elasticity component balances the contractile force

by pulling the eye globe with the same force T_{MR} .

$$T_{MR} = -K_{SE}(\theta_{SE_{MR}} - \Delta\theta_{SE_{MR}}) \quad (94)$$

Equations 93 and 94 and can be combined into the equation:

$$-F_{MR} - K_{LT}(\theta_{LT_{MR}} + \Delta\theta_{LT_{MR}}) + (-B_{AG}\Delta\dot{\theta}_{LT_{MR}}) = -K_{SE}(\theta_{SE_{MR}} - \Delta\theta_{SE_{MR}}) \quad (95)$$

This equation is similar to Equation 81, except that in the case of Equation 95 the B_{AG} is used, and in case of Equation 81 B_{ANT} is used.

$$K_{SE}(\theta_{SE_{MR}} + \Delta\theta_{SE_{MR}}) - F_{MR} - K_{LT}(\theta_{LT_{MR}} + \Delta\theta_{LT_{MR}}) - B_{ANT}\Delta\dot{\theta}_{LT_{MR}} = 0 \quad (81)$$

Following the computational steps similar to those performed in Section A.2 for Equation 81 it is possible to derive the following two equations from Equation 95.

$$T_{MR} = -K_{SE}(\Delta\theta - \Delta\theta_{LT_{MR}}) \quad (96)$$

$$T_{MR} = -\hat{F}_{MR} - K_{LT}\Delta\theta_{LT_{MR}} - \hat{B}_{AG}\Delta\dot{\theta}_{LT_{MR}} \quad (97)$$

combining Equations 96 and 97, Equation 31 can be derived:

$$K_{SE}(\Delta\theta - \Delta\theta_{LT_{MR}}) = \frac{\hat{F}_{MR}K_{SE}}{K_{SE} + K_{LT}} + \frac{\Delta\theta K_{SE}K_{LT}}{K_{SE} + K_{LT}} + \hat{B}_{AG}\Delta\dot{\theta}_{LT_{MR}} \quad (31)$$

Antagonist Muscle Mechanical Model of Lateral Rectus

The antagonist muscle is stretched by the agonist pull. Assuming that the lateral rectus plays the role of the antagonist, the MMM of the medial rectus being stretched in the positive direction is presented in Fig. 27. Originally the length of the displacement in the series elasticity and length tension springs added together is θ_{LR} . The value of θ_{LR} increases when the eye moves to the right by $\Delta\theta$. $\Delta\theta$ is represented by

a negative value measured in degrees. Thus the resulting displacement of θ_{MR} is $\theta_{MR} - \Delta\theta$. Both the length tension and series elasticity components lengthen as a result of the agonist pull. The eye rotation $\Delta\theta$ can be split into the displacement of the series elasticity component and the length tension component: $\Delta\theta = \Delta\theta_{SE_MR} + \Delta\theta_{LT_MR}$. Both $\Delta\theta_{SE_MR}$ and $\Delta\theta_{LT_MR}$ are negative values. The resulting displacement of the series elasticity component is $\theta_{SE_MR} - \Delta\theta_{SE_MR}$ and the length tension component is $\theta_{LT_MR} - \Delta\theta_{LT_MR}$. The damping component modeling force velocity relationship $-B_{ANT} \Delta\dot{\theta}_{LT_MR}$ resists the muscle stretching. The negative sign in front of the damping component makes positive the value of force represented by $B_{AG} \Delta\dot{\theta}_{LT_LR}$. The amount of resistive force is based upon the velocity of stretching of the length tension component.

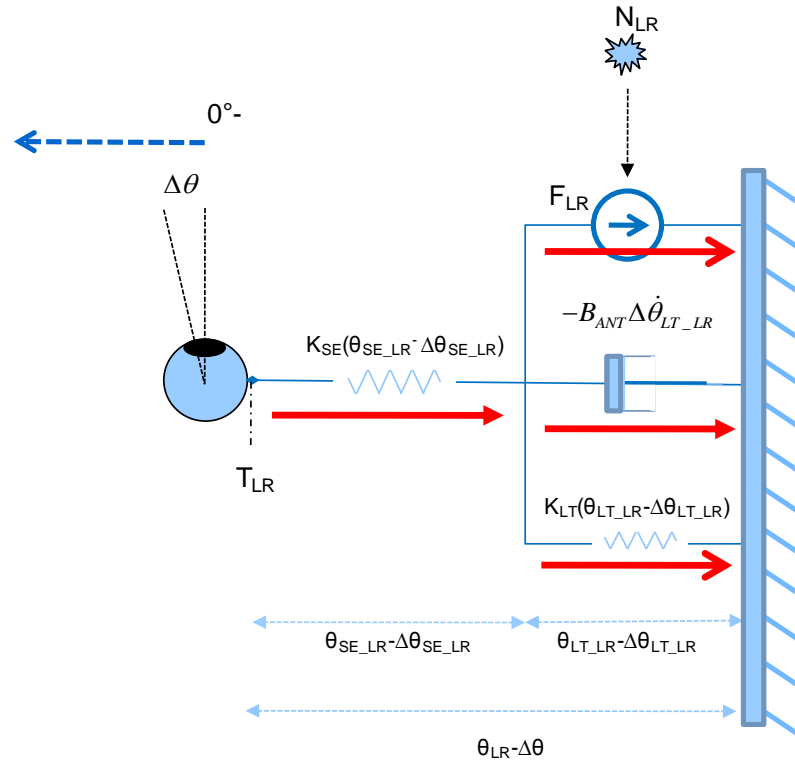


Fig. 27. Antagonist Muscle Mechanical Model of Lateral Rectus. Arrows represent the direction of the forces.

Using Fig. 27, we can write the equation of force with which the part of the diagram responsible for contraction (active state tension, damping component, length tension component) pulls the series elasticity component.

$$T_{LR} = F_{LR} + K_{LT}(\theta_{LT_LR} - \Delta\theta_{LT_LR}) + (-B_{ANT}\Delta\dot{\theta}_{LT_LR}) \quad (98)$$

Resisting the contraction series elasticity component balances the contractile force by pulling the eye globe with the same force T_{LR} .

$$T_{LR} = K_{SE}(\theta_{SE_LR} - \Delta\theta_{SE_LR}) \quad (99)$$

Equations 98 and 99 can be combined into the equation:

$$F_{LR} + K_{LT}(\theta_{LT_LR} - \Delta\theta_{LT_LR}) + (-B_{ANT}\Delta\dot{\theta}_{LT_LR}) = K_{SE}(\theta_{SE_LR} - \Delta\theta_{SE_LR}) \quad (100)$$

This equation is similar to Equation 70, except that in case of Equation 100 the B_{ANT} is used, and in case of Equation 70 B_{AG} is used.

$$-K_{SE}(\theta_{SE_{LR}} + \Delta\theta_{SE_{LR}}) + F_{LR} + K_{LT}(\theta_{LT_{LR}} - \Delta\theta_{LT_{LR}}) - B_{AG}\Delta\dot{\theta}_{LT_{LR}} = 0 \quad (70)$$

Following the computational steps similar to those performed in Section A.2 for Equation 70 it is possible to derive the following two equations from Equation 100.

$$T_{LR} = K_{SE}(\Delta\theta_{LT_{LR}} - \Delta\theta) \quad (101)$$

$$T_{LR} = \frac{\hat{F}_{LR}K_{SE}}{K_{SE} + K_{LT}} - \frac{\Delta\theta K_{SE}K_{LT}}{K_{SE} + K_{LT}} - \hat{B}_{ANT}\Delta\dot{\theta}_{LT_{LR}} \quad (102)$$

Combining Equations 101 and 102 Equation 30 can be derived:

$$K_{SE}(\Delta\theta_{LT_{LR}} - \Delta\theta) = \frac{\hat{F}_{LR}K_{SE}}{K_{SE} + K_{LT}} - \frac{\Delta\theta K_{SE}K_{LT}}{K_{SE} + K_{LT}} - \hat{B}_{ANT}\Delta\dot{\theta}_{LT_{LR}} \quad (30)$$

Oculomotor Plant Mechanical Model Equations

The diagram accounting for all of the forces inside of the horizontal OPMM during a saccade of negative amplitude is presented in Fig. 28.

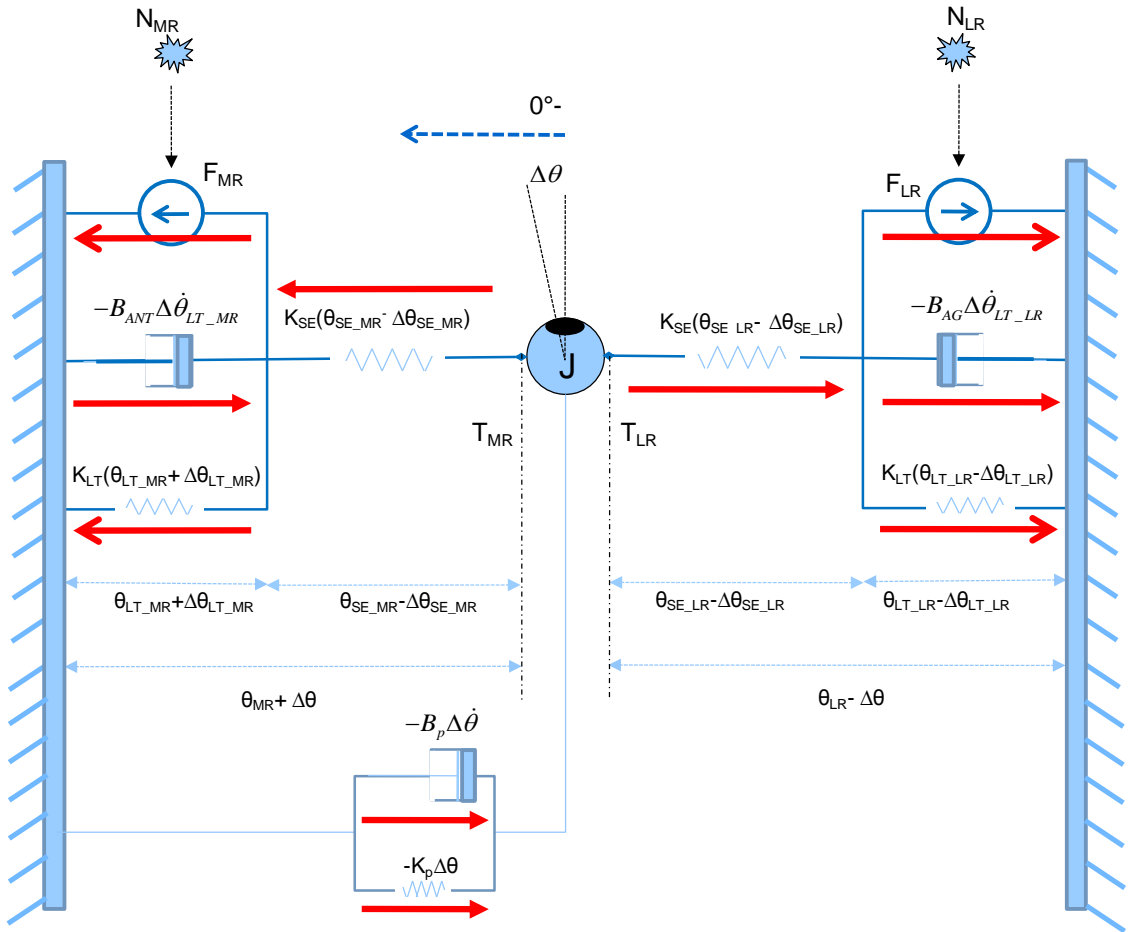


Fig. 28. The Oculomotor Plant Mechanical Model generating negative amplitude saccades. Arrows show the direction of forces for each component. F_{LR} , F_{MR} – active state tension; K_{LT} – length tension coefficient; K_{SE} – series elasticity coefficient; $\theta_{SE_MR} - \Delta\theta_{SE_MR}$, $\theta_{SE_LR} - \Delta\theta_{SE_LR}$ – length of the displacement of the series elasticity component of each muscle; $\theta_{LT_MR} + \Delta\theta_{LT_MR}$, $\theta_{LT_LR} - \Delta\theta_{LT_LR}$ – length of the displacement of the length tension component of each muscle; $\Delta\dot{\theta}_{LT_LR}$, $\Delta\dot{\theta}_{LT_MR}$ – velocity of change of the length tension component of the lateral and the medial recti; B_{AG} , B_{ANT} – damping coefficients for the agonist (the lateral rectus) and the antagonist (the medial rectus), $\Delta\theta$ – eye rotation; K_p – combined passive elasticity coefficient of the eye-orbit, both muscles and surrounding tissues; B_p – damping component coefficient for the viscosity of the eye-orbit and surrounding tissues. J is the rotational inertia of the eye globe.

Applying Newton's second law the sum of all forces acting on the eye globe equals the acceleration of the eye globe multiplied by the inertia of the eye globe.

$$J\Delta\ddot{\theta} = T_{LR} - T_{MR} + (-K_p\Delta\theta) + (-B_p\Delta\dot{\theta}) \quad (103)$$

Where J - eye globe's inertia, $\Delta\theta$ - eye rotation, $\Delta\dot{\theta}$ velocity of the eye rotation, $\Delta\ddot{\theta}$ eye rotation acceleration. The negative sign in front of the damping component $B_p\Delta\dot{\theta}$ and the passive elasticity component $K_p\Delta\theta$ makes positive the value of forces represented by $B_p\Delta\dot{\theta}$ and $K_p\Delta\theta$. T_{LR} can be calculated by Equation 101 and T_{MR} can be calculated by Equation 96.

Thus Equation 103 can be rewritten in the form of Equation 32:

$$J\Delta\ddot{\theta} = K_{SE}(\Delta\theta_{LT_LR} - \Delta\theta) - K_{SE}(\Delta\theta - \Delta\theta_{LT_MR}) + K_p\Delta\theta + B_p\Delta\dot{\theta} \quad (32)$$

A.4 Oculomotor Plant Kalman Filter

Equation 29 can be rewritten as Equation 45

$$\dot{x}_1(t) = x_4(t) \quad (45)$$

approximating the derivative as $\dot{x}(k) = \frac{x(k+1) - x(k)}{\Delta\rho}$ Equation 45 can be rewritten

as:

$$\frac{x_1(k+1) - x_1(k)}{\Delta\rho} = x_4(k) \quad (104)$$

$$x_1(k+1) = x_1(k) + x_4(k)\Delta\rho \quad (105)$$

$$x_1(k+1) = x_1(k) + \mathbf{0} \cdot x_2(k) + \mathbf{0} \cdot x_3(k) + x_4(k)\Delta\rho + \mathbf{0} \cdot x_5(k) + \mathbf{0} \cdot x_6(k) \quad (106)$$

Equation 106 creates the first line of the matrix A_k .

To derive the Equation 46 from the Equation 25 following steps are taken:

$$K_{SE}(x_2(k) - x_1(k)) = \frac{K_{SE}x_5(k)}{K_{LT} + K_{SE}} - \frac{K_{LT}K_{SE}x_1(k)}{K_{LT} + K_{SE}} - \hat{B}_{AG}\dot{x}_2(k) \quad (107)$$

$$\hat{B}_{AG}\dot{x}_2(k) = \frac{K_{SE}x_5(k)}{K_{LT} + K_{SE}} - \frac{K_{LT}K_{SE}x_1(k)}{K_{LT} + K_{SE}} - K_{SE}x_2(k) + K_{SE}x_1(k) \quad (108)$$

$$\hat{B}_{AG}\dot{x}_2(k) = \frac{K_{SE}}{K_{LT} + K_{SE}}x_5(k) + \left(K_{SE} - \frac{K_{LT}K_{SE}}{K_{LT} + K_{SE}} \right)x_1(k) - K_{SE}x_2(k) \quad (109)$$

$$\hat{B}_{AG}\dot{x}_2(k) = \frac{K_{SE}^2}{K_{LT} + K_{SE}}x_1(k) - K_{SE}x_2(k) + \frac{K_{SE}}{K_{LT} + K_{SE}}x_5(k) \quad (110)$$

$$\dot{x}_2(k) = \frac{K_{SE}^2}{\hat{B}_{AG}(K_{LT} + K_{SE})}x_1(k) - \frac{K_{SE}}{\hat{B}_{AG}}x_2(k) + \frac{K_{SE}}{\hat{B}_{AG}(K_{LT} + K_{SE})}x_5(k) \quad (46)$$

approximating derivative as $\dot{x}(k) = \frac{x(k+1) - x(k)}{\Delta\rho}$ the Equation 46 can be rewritten as:

$$x_2(k+1) - x_2(k) = \frac{\Delta\rho K_{SE}^2}{\hat{B}_{AG}(K_{LT} + K_{SE})}x_1(k) - \frac{\Delta\rho K_{SE}}{\hat{B}_{AG}}x_2(k) + \frac{\Delta\rho K_{SE}}{\hat{B}_{AG}(K_{LT} + K_{SE})}x_5(k) \quad (111)$$

$$x_2(k+1) = \frac{\Delta\rho K_{SE}^2}{\hat{B}_{AG}(K_{LT} + K_{SE})}x_1(k) + \left(1 - \frac{\Delta\rho K_{SE}}{\hat{B}_{AG}} \right)x_2(k) + \frac{\Delta\rho K_{SE}}{\hat{B}_{AG}(K_{LT} + K_{SE})}x_5(k) \quad (112)$$

$$x_2(k+1) = \frac{\Delta\rho K_{SE}^2}{\hat{B}_{AG}(K_{LT} + K_{SE})} x_1(k) + \left(1 - \frac{\Delta\rho K_{SE}}{\hat{B}_{AG}}\right) x_2(k) + 0 \cdot x_3(k) + 0 \cdot x_4(k) + \frac{\Delta\rho K_{SE}}{\hat{B}_{AG}(K_{LT} + K_{SE})} x_5(k) + 0 \cdot x_6(k) \quad (113)$$

Equation 113 creates the second line of the matrix A_k .

Similar steps can be taken to derive Equation 47 from Equation 26. Finally Equation 47 can be presented in the following form:

$$x_3(k+1) = \frac{\Delta\rho K_{SE}^2}{\hat{B}_{ANT}(K_{LT} + K_{SE})} x_1(k) + 0 \cdot x_2(k) + \left(1 - \frac{\Delta\rho K_{SE}}{\hat{B}_{ANT}}\right) x_3(k) + 0 \cdot x_4(k) + 0 \cdot x_5(k) - \frac{\Delta\rho K_{SE}}{\hat{B}_{ANT}(K_{LT} + K_{SE})} x_6(k) \quad (114)$$

Equation 114 creates the third line of the matrix A_k .

To derive Equation 48 from Equation 28 the following steps are taken:

$$K_{SE}(x_2(k) - x_1(k)) - K_{SE}(x_1(k) - x_3(k)) = K_p x_1(k) + B_p \cdot x_4(k) + J \cdot \dot{x}_4(k) \quad (115)$$

$$K_{SE} \cdot x_2(k) + K_{SE} \cdot x_3(k) = (K_p + 2K_{SE}) \cdot x_1(k) + B_p \cdot x_4(k) + J \cdot \dot{x}_4(k) \quad (116)$$

$$J \cdot \dot{x}_4(k) = K_{SE} \cdot x_2(k) + K_{SE} \cdot x_3(k) - (K_p + 2K_{SE}) \cdot x_1(k) - B_p \cdot x_4(k) \quad (117)$$

$$\dot{x}_4(k) = \frac{K_{SE}}{J} \cdot x_2(k) + \frac{K_{SE}}{J} \cdot x_3(k) - \frac{(K_p + 2K_{SE})}{J} \cdot x_1(k) - \frac{B_p}{J} \cdot x_4(k) \quad (48)$$

approximating the derivative as $\dot{x}(k) = \frac{x(k+1) - x(k)}{\Delta\rho}$ Equation 48 can be rewritten as:

$$x_4(k+1) - x_4(k) = \Delta\rho \frac{K_{SE}}{J} \cdot x_2(k) + \Delta\rho \frac{K_{SE}}{J} \cdot x_3(k) - \Delta\rho \frac{(K_p + 2K_{SE})}{J} \cdot x_1(k) - \Delta\rho \frac{B_p}{J} \cdot x_4(k) \quad (118)$$

$$x_4(k+1) = \Delta\rho \frac{K_{SE}}{J} \cdot x_2(k) + \Delta\rho \frac{K_{SE}}{J} \cdot x_3(k) - \Delta\rho \frac{(K_p + 2K_{SE})}{J} \cdot x_1(k) + \left(1 - \Delta\rho \frac{B_p}{J}\right) \cdot x_4(k) \quad (119)$$

$$x_4(k+1) = -\Delta\rho \frac{(K_p + 2K_{SE})}{J} + \Delta\rho \frac{K_{SE}}{J} \cdot x_2(k) + \Delta\rho \frac{K_{SE}}{J} \cdot x_3(k) + \left(1 - \Delta\rho \frac{B_p}{J}\right) \cdot x_4(k) + 0 \cdot x_5(k) + 0 \cdot x_6(k) \quad (120)$$

Equation 120 creates the fourth line of the matrix A_k .

To calculate Equation 49 Equation 21 can be rewritten as:

$$\dot{x}_5(t) = \frac{N_{AG} - x_5(t)}{\tau_{AG}} \quad (49)$$

approximating the derivative as $\dot{x}(k) = \frac{x(k+1) - x(k)}{\Delta\rho}$ Equation 49 can be rewritten

as:

$$x_5(k+1) - x_5(k) = \Delta\rho \frac{N_{LR}}{\tau_{AG}} - \Delta\rho \frac{x_5(k)}{\tau_{AG}} \quad (121)$$

$$x_5(k+1) = \Delta\rho \frac{N_{LR}}{\tau_{AG}} + \left(1 - \frac{\Delta\rho}{\tau_{AG}}\right) x_5(k) \quad (122)$$

$$x_5(k+1) = 0 \cdot x_1(k) + 0 \cdot x_2(k) + 0 \cdot x_3(k) + 0 \cdot x_4(k) + \left(1 - \frac{\Delta\rho}{\tau_{AG}}\right) \cdot x_5(k) + 0 \cdot x_6(k) + \Delta\rho \frac{N_{LR}}{\tau_{AG}} \quad (123)$$

Equation 123 creates the fifth line of the matrix A_k and control vector u_k .

To calculate Equation 50 Equation 22 can be rewritten as:

$$\dot{x}_6(t) = \frac{N_{ANT} - x_6(t)}{\tau_{ANT}} \quad (50)$$

approximating derivative as $\dot{x}(k) = \frac{x(k+1)-x(k)}{\Delta\rho}$ Equation 50 can be rewritten as:

$$x_6(k+1) = 0 \cdot x_1(k) + 0 \cdot x_2(k) + 0 \cdot x_3(k) + 0 \cdot x_4(k) + 0 \cdot x_5(k) + \left(1 - \frac{\Delta\rho}{\tau_{ANT}}\right) \cdot x_6(k) + \Delta\rho \frac{N_{MR}}{\tau_{ANT}} \quad (124)$$

Equation 124 creates the sixth line of the matrix A_k and control vector u_k .

Equations 106, 113, 114, 120, 123, and 124 can be re-written in a matrix form as required for Kalman Filtering by Equation 36. Fig. 29 presents the result.

$$\begin{array}{c}
 \begin{pmatrix} x_1(k+1) \\ x_2(k+1) \\ x_3(k+1) \\ x_4(k+1) \\ x_5(k+1) \\ x_6(k+1) \end{pmatrix} = \begin{pmatrix} 1 & 0 & 0 & \Delta\rho & 0 & 0 \\ \Delta\rho \frac{K_{SE}^2}{B_{AG}(K_{LT} + K_{SE})} \left(1 - \Delta\rho \frac{K_{SE}}{B_{AG}}\right) & 0 & 0 & 0 & \Delta\rho \frac{K_{SE}}{B_{AG}(K_{LT} + K_{SE})} & 0 \\ \Delta\rho \frac{K_{SE}^2}{B_{ANT}(K_{LT} + K_{SE})} & 0 & \left(1 - \Delta\rho \frac{K_{SE}}{B_{ANT}}\right) & 0 & 0 & -\Delta\rho \frac{K_{SE}}{B_{ANT}(K_{LT} + K_{SE})} \\ \Delta\rho \frac{2K_{SE} + K_p}{J} & \Delta\rho \frac{K_{SE}}{J} & \Delta\rho \frac{K_{SE}}{J} & 1 - \Delta\rho \frac{B_p}{J} & 0 & 0 \\ 0 & 0 & 0 & 0 & \left(1 - \frac{\Delta\rho}{\tau_{AG}}\right) & 0 \\ 0 & 0 & 0 & 0 & 0 & \left(1 - \frac{\Delta\rho}{\tau_{ANT}}\right) \end{pmatrix} \begin{pmatrix} x_1(k) \\ x_2(k) \\ x_3(k) \\ x_4(k) \\ x_5(k) \\ x_6(k) \end{pmatrix} + \begin{pmatrix} 1 & 0 & 0 & 0 & 0 & 0 \\ 0 & 1 & 0 & 0 & 0 & 0 \\ 0 & 0 & 1 & 0 & 0 & 0 \\ 0 & 0 & 0 & 1 & 0 & 0 \\ 0 & 0 & 0 & 0 & 1 & 0 \\ 0 & 0 & 0 & 0 & 0 & 1 \end{pmatrix} \begin{pmatrix} 0 \\ 0 \\ 0 \\ \Delta t \frac{N_{LR}}{\tau_{AG}} \\ \Delta t \frac{N_{MR}}{\tau_{AG}} \\ \Delta t \frac{N_{MR}}{\tau_{ANT}} \end{pmatrix}
 \end{array}$$

Transition Matrix
Control Matrix
Control Vector

State Vector
State Vector
Control Vector

Fig. 29. State vector prediction by the OPKF, during a saccade of a positive amplitude.